Received: 28 September 2023 | Revised: 27 January 2024 | Accepted: 31 January 2024
DOI: 10.1002/joc.8395

RESEARCH ARTICLE

International Journal of Climatology RMetS

Supercell precipitation contribution to the United States hydroclimate

Aaron W. Zeeb | **Walker S. Ashley** | **Alex M. Haberlie** | **Vittorio A. Gensini** | **Allison C. Michaelis**

Department of Earth, Atmosphere, and Environment, Northern Illinois University, DeKalb, Illinois, USA

Correspondence
Walker S. Ashley, Department of Earth, Atmosphere, and Environment, Northern Illinois University, DeKalb, IL, USA.
Email: washley@niu.edu

Funding information
National Science Foundation Awards, Grant/Award Numbers: 1637225, 1800582; National Oceanic and Atmospheric Administration Award, Grant/Award Number: NA22OAR4690645

Abstract

This research seeks to understand simulated supercell precipitation characteristics across the conterminous United States (CONUS) using high-resolution, convection-permitting, dynamically downscaled simulations for three 15-year epochs. Epochs include a historical end-of-20th-century period (1990–2005) and two end-of-21st-century (2085–2100) scenarios for intermediate and pessimistic greenhouse gas concentration trajectories. Simulated updraft helicity, which measures the corkscrew flow within a storm's updraft, is used as a proxy for supercells. An algorithm tracks and catalogues updraft helicity swaths that, when buffered, are used to acquire simulated precipitation from supercells. The historical epoch provides a baseline climatology of supercell precipitation for a contemporary climate, which is then compared against the two future epochs to assess how supercell precipitation may change during the 21st century. Despite their relatively small size, supercells provide critical precipitation to the Wheat and Corn Belts, large expanses of CONUS pasture and rangeland, regional aquifers and several large river basins. Many areas in the central CONUS receive upwards of 3%–6% of their annual and 5%–8% of their warm-season precipitation from these storms. Results suggest that precipitation contribution from supercells will decrease in the future across most of the High Plains and Central and Northern Great Plains with robust increases likely across the south-central and Southeast regions. Supercell precipitation rates are expected to increase for large portions of the CONUS by the end-of-the-21st-century, suggesting a growing threat for flash floods from these storms as they become more efficient precipitation producers. This research provides an initial perspective on the magnitude of supercell precipitation and potential changes to this important hydrologic input to assist water-sensitive industries, private and public insurance markets, agriculture entities, as well as inform plans to mitigate and build resilience to rapid environmental and societal change.

KEYWORDS
climate change, climate models, climatology, extreme events, hydrometeorology, precipitation, rainfall, supercells

1 | INTRODUCTION

The world record precipitation rate on a 2–3-h time scale occurred from the D'Hannis, TX supercell on 31 May 1935, which produced 559 mm of precipitation in just 2.75 h (Doswell, 1998; Smith et al., 2001, 2018; WMO, 1986). Decades later, the first billion-dollar thunderstorm in the United States occurred when a supercell travelled over the Dallas-Fort Worth metropolitan area on 5 May 1995 (Doswell, 1998; NOAA, 1995; Smith et al., 2001). The flash flooding from this supercell, which killed 16, was caused by exceptional short-term precipitation rates that transpired at 5- ($231\ mm\cdot h^{-1}$), 15- ($210\ mm\cdot h^{-1}$), and 60-min ($115\ mm\cdot h^{-1}$) intervals. Another example of a supercell producing extreme precipitation rates took place in Orlando, FL on 26 March 1992. This storm produced a peak 1-min precipitation rate of $330\ mm\cdot h^{-1}$ (Doswell, 1998; Smith et al., 2001). More recently, on 12 April 2023, a stationary supercell produced over 650 mm of rainfall in 12 h over Fort Lauderdale, FL, with a 10-min maximum rainfall of 38 mm (Bacon and Ortiz, 2023; Ebrahimji et al., 2023; Ives & Hauser, 2023). These cases illustrate that supercells can produce dangerous amounts of precipitation resulting from some of the most extreme short-term precipitation rates compared to other morphologies (Beatty et al., 2008; Bunkers & Doswell, 2016; Doswell, 1998; Doswell et al., 1996; Duda & Gallus, 2010; Giordano & Fritsch, 1991; Nielsen et al., 2015; Rogash & Racy, 2002; Rogash & Smith, 2000; Smith et al., 2001, 2018).

Supercell events are characterized by two factors that can lead to extreme precipitation rates (Doswell et al., 1996)—namely, (1) they are long-lasting; and (2) they often form in environments that permit enhanced precipitation production (Beatty et al., 2008; Doswell, 1998; Doswell et al., 1996; Hitchens & Brooks, 2013; Moller et al., 1990, 1994). This situation is particularly common for one of the three supercell archetypes known as the high-precipitation (HP) supercell, which is the dominant morphology across the eastern CONUS (Moller et al., 1994). HP supercell precipitation is enhanced by a rather large and robust updraft and affiliated mesocyclone permitting significant amounts of water vapour to be ingested, thus, enhancing precipitation production (Beatty et al., 2008; Doswell et al., 1996; Moller et al., 1994). Furthermore, supercell precipitation can be enhanced through rotation generated by strong low-level shear, boosting precipitation production through dynamic lift from vertical perturbation pressure gradient forces. The dynamic lift maximizes precipitation rates by enhancing the updraft and lifting what is otherwise negatively buoyant air to its level of free convection (LFC). Moreover, the strong low-level rotation associated with supercells can enhance warm rain formation and increase precipitation efficiency and production (Nielsen & Schumacher, 2018, 2020a). Precipitation production can be further aided by a low-level warm and moist air stream—roughly bounded by the lifting condensation level (LCL) and 4-km above ground level (AGL)—that intensifies precipitation formation (Jo & Lasher-Trapp, 2022). Conversely, dry mid-levels can affect the overall structure, strength and longevity of a supercell through entrainment and subsequent evaporation and sublimation of precipitation (e.g., Grant & van den Heever, 2014; Morrison, 2017; Lasher-Trapp et al., 2021; Jo & Lasher-Trapp, 2022, 2023; Morrison et al., 2022; LeBel & Markowski, 2023). The extent of how detrimental this dry air is on a supercell depends on the near storm environment (e.g., the height, depth and 'dryness' of the dry layer(s)), which varies spatiotemporally throughout the CONUS and a supercell's lifecycle. Additionally, the width of a supercell's updraft, determined by entrainment CAPE (ECAPE; Zhang, 2009; Peters, Morrison, et al., 2020; Peters, Nowotarski, et al., 2020; Peters et al., 2022), also controls the impacts of dry air where often wider updrafts are more resistant to entrainment (e.g., LeBel & Markowski, 2023; Morrison, 2017; Morrison et al., 2022; Peters et al., 2019; Peters et al., 2022; Peters, Morrison, et al., 2020; Peters, Nowotarski, et al., 2020; Zhang, 2009).

Through the Clausius-Clapeyron relationship, the increasing temperatures of the Earth's oceans and troposphere are causing higher rates of evaporation, leading to a greater amount of water vapour in the atmosphere; however, this relationship breaks down over land (e.g., Held & Soden, 2006; Trenberth, 1999). An increase in water vapour may result in the modification of precipitation patterns including changes in precipitation rates, with some regions experiencing increased intensities and durations of precipitation events (Allen & Ingram, 2002; Del Genio et al., 2007; Diffenbaugh et al., 2005; Fowler et al., 2021; Kendon et al., 2012, 2014; Kirtman et al., 2013; Kunkel et al., 2013; Meehl et al., 2005; Min et al., 2009, 2011; O'Gorman & Schneider, 2009; Pall et al., 2007; Prein, Liu, et al., 2017; Prein, Rasmussen, et al., 2017; Rasmussen et al., 2020; Reidmiller et al., 2018; Sheffield & Wood, 2008; Tebaldi et al., 2006; Trenberth et al., 2003). With amplified precipitation rates and longer durations, flash flooding—the deadliest and most destructive storm hazard in the CONUS (Ashley & Ashley, 2008)—is also expected to become more frequent (Collins et al., 2013; Dai et al., 2018; Hirabayashi et al., 2013; Koirala et al., 2014). A common source of flooding is extreme precipitation events, which are projected to be more frequent under a warming climate, likely resulting in greater annual and seasonal precipitation tallies in the future (Attema et al., 2014; Ban et al., 2015; Bao et al., 2015; Donat et al., 2016; Gutowski et al., 2008; Karl & Trenberth, 2003; Meehl et al., 2005; Min et al., 2011; Muller et al., 2011; O'Gorman & Schneider, 2009; Prein, Liu, et al., 2017; Zhu, 2013; Zhu et al., 2013).

Over the last two decades, research has sought to determine how anthropogenic climate change (ACC) affects severe convective storms (SCSs). Results suggest an overall increase in days supportive for SCSs in the future; however, the distribution of SCS populations may vary due to changes in forcing, moisture, convective inhibition (CIN), overlapping of ingredients (e.g., CIN with convective available potential energy [CAPE]), convection initiation and overall sustenance of SCSs (Ashley et al., 2023; Hoogewind et al., 2017; Pilguj et al., 2022; Taszarek et al., 2021). Research suggests SCSs and their associated severe perils will be more frequent and intense with an expansion in their seasonality by the end-of-the-21st-century (Trapp et al., 2011, 2019; Gensini & Mote, 2014, 2015; Trapp & Hoogewind, 2016; Hoogewind et al., 2017; Rasmussen et al., 2020; Gensini, 2021; Ashley et al., 2023). Should these projections come to fruition, a plethora of environmental and societal factors such as habitation loss, economic cost and casualties, will be at risk.

Despite previous research into supercells and their precipitation, to our knowledge, no work has constructed a long-term climatology of supercell precipitation. Additionally, while studies have sought to understand historical and future changes to extreme precipitation (see reviews by Kunkel et al., 2013; Prein, Liu, et al., 2017; Prein, Rasmussen, et al., 2017; Reidmiller et al., 2018) along with SCSs and their environments (see reviews by Brooks, 2013; Tippett et al., 2015; Allen, 2018; Gensini, 2021), no efforts have explored the precipitation produced specifically by supercells from a climate change perspective. For these reasons, this study employs convection-permitting, dynamically downscaled simulation output to assess how ACC may affect supercell precipitation in the CONUS by comparing two end-of-21st-century scenarios to a late 20th-century epoch. We seek to determine the contribution of supercells to the overall hydroclimate of the CONUS, assess potential future spatiotemporal changes to these contributions and evaluate changes in storm-based precipitation metrics due to a warming climate.

2 | DATA AND METHODS

2.1 | Simulation output

The convection-permitting, dynamically downscaled regional climate model (CP-RCM) output used in this research were obtained from Gensini et al. (2023). Gensini et al. (2023) used bias-corrected output from the National Center for Atmospheric Research's (NCAR) Community Earth System Model (CESM; Hurrell et al., 2013; Bruyère et al., 2014) Coupled Model Intercomparison Project phase 5 (CMIP5; Taylor et al., 2012) general circulation model (GCM) as CP-RCM initial and lateral boundary conditions. Bias correction assists in reducing errors produced by GCMs that may be passed to the CP-RCM through dynamically downscaling (Christensen et al., 2008), resulting in overall performance improvement (Christensen et al., 2008; Gensini et al., 2023; Ines & Hansen, 2006). The advanced research core of the Weather Research and Forecasting model (WRF-ARW) v.4.1.2 (Skamarock et al., 2019) was then run with a spatial extent encompassing the CONUS at a horizontal grid spacing of 3.75 km, 51 vertical levels and temporal output at every 15 min. Hereafter, the CP-RCM used in this research is referred to as WRF-BCC (WRF-Bias Corrected CESM). Detailed information on the simulations, as well as verification of the output, may be found in Gensini et al. (2023).

The end-of-21st-century (2085–2100) simulation period employs the CESM data for Representative Concentration Pathways (RCP; Moss et al., 2010) 4.5 and 8.5 to analyse and compare outcomes under the intermediate (RCP4.5) and extreme/pessimistic (RCP8.5) emissions scenarios, which have been used in Intergovernmental Panel on Climate Change (IPCC) reports (e.g., IPCC, 2014). Simulations were continuously integrated with spectral nudging (Gensini et al., 2023; Miguez-Macho et al., 2004) at 6-h intervals throughout the entire integration period (1 October–30 September) and reinitialized annually to better simulate conditions that rely on hydrologic memory (Chen & Kumar, 2002; Christian et al., 2015; Gensini et al., 2023; Giorgi & Mearns, 1999). Overall, 45 simulations were created for the three 15-year epochs; herein, these are referred to as HIST (1990–2005), FUTR 4.5 (RCP4.5, 2085–2100) and FUTR 8.5 (RCP8.5, 2085–2100).

As demonstrated by Gensini et al. (2023), HIST recreated historical temperature and precipitation patterns well, with a few regional and seasonal biases compared to assimilated observational data (i.e., PRISM), including a dry precipitation bias during the June–August period in the Southeast. In the Great Plains, which observes the highest count of supercells partially due to the thermodynamics driven by low-level heat and moisture, the warm and dry biases in HIST are less severe compared to prior dynamically downscaled simulations (Ashley et al., 2023; Haberlie & Ashley, 2019a; Liu et al., 2017; Rasmussen et al., 2020). Precipitation biases for the HIST may be summarized as including a: (1) wet bias in the northern Plains, High Plains and Intermountain West during December–February; (2) warm-season

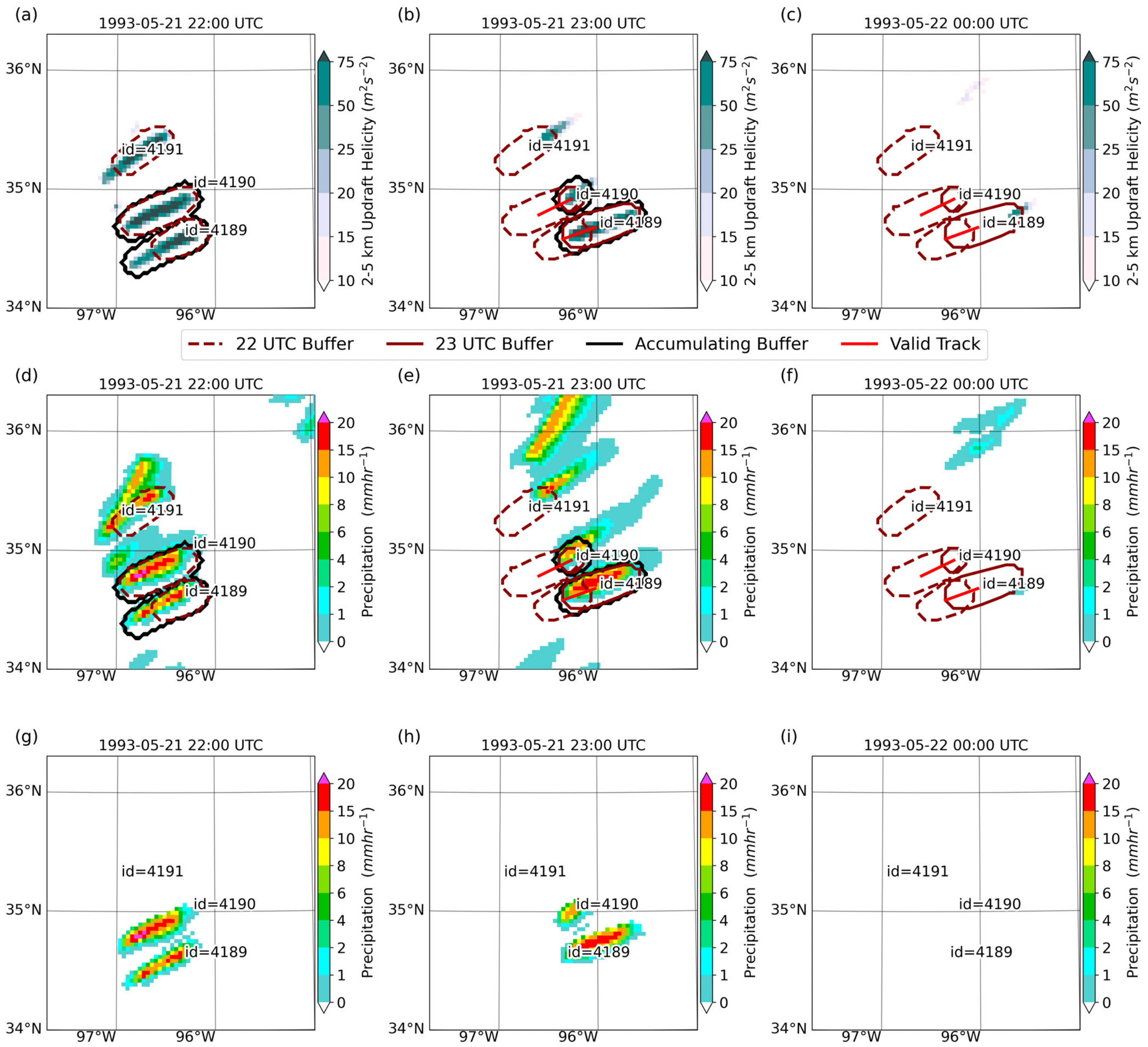

FIGURE 1 Method used to accumulate UH75 supercell precipitation in simulation output. (a)–(c) Demonstrate the method for segmenting, tracking and cataloguing supercells. A 10-km buffer (dashed dark red line for 22 UTC and solid dark red line for 23 UTC) is placed around hourly max 2–5 km UH (coloured pixels) that exceed 75 $m^2 \cdot s^{-2}$. Each hour 'slice' is segmented and assigned a unique label where regions are connected in time by checking for spatial overlap between two consecutive hours, or slices. The valid overlapping slices are then concatenated to form a valid 'swath'', or footprint, of a supercell. Only tracks lasting at least 2 h are retained for analysis, which is shown by red track lines. A new 10-km buffer (used for accumulation) is built around each valid track by extending the 'swath' to include the surrounding UH pixels that exceed 50 $m^2 \cdot s^{-2}$ (black solid line). (d)–(f) Illustrates the precipitation data (coloured pixels) for the corresponding hour and is masked over each new buffer to 'cut' the associated supercell precipitation. (g)–(i) Reveal the resulting accumulated precipitation for each valid track, which is catalogued with the corresponding unique id number for each supercell. [Colour figure can be viewed at wileyonlinelibrary.com]

dry bias in the Southeast, Mid-Atlantic and Northeast CONUS; and (3) dry bias in the Intermountain West during the climatological peak of monsoon season (Gensini et al., 2023). Additionally, WRF-BCC—unlike a pseudo-global warming approach—includes changes associated with general circulation and modes of climate variability (cf. Chap. 4 in IPCC, 2021) that may modify the environments and ingredients supportive for SCSs.

2.2 | Updraft helicity

Updraft helicity (UH) is a diagnostic variable in simulations that represents rotating storm updrafts that is frequently used to predict storm-scale rotation and associated severe weather (Ashley et al., 2023; Potvin & Flora, 2015; Sobash et al., 2011; Sobash & Kain, 2017; Sobash, Romine, et al., 2016; Sobash, Schwartz, et al., 2016). UH is calculated by taking the vertical integral of the product of vertical vorticity and vertical velocity (see Kain et al. (2008) for derivation). In this research, the layer between 2 and 5 km AGL, which accounts for the low-to-middle portions of a typical convective cell, is used to detect the presence of a deep, persistent, 'midlevel' mesocyclone, which defines a supercell. Midlevel mesocyclones are produced by horizontal vorticity generated from the tilting of environmental wind shear into the vertical via the tilting term in the vorticity equation (Markowski & Richardson, 2010).

2.3 | Identifying and tracking supercells

Identifying and tracking supercells in the WRF-BCC output follows the procedure described in Ashley et al. (2023) where UH tracks—a surrogate of supercells within simulations (Sobash et al., 2011; Naylor et al., 2012; Potvin & Flora, 2015; Gallo et al., 2016; Sobash, Rominem et al., 2016; Sobash, Schwartz, et al., 2016; Sobash & Kain, 2017)—are used to identify, track, label and compile UH 'swaths' (Figure 1a–c). Such swaths are the basic outlines of supercells based on UH intensity, spatial and temporal thresholds. Supercell swaths are first outlined by removing all values of hourly maximum 2–5 km AGL UH $<75\ m^2{\cdot}s^{-2}$, retaining values of $\geq 75\ m^2{\cdot}s^{-2}$, which are then segmented and assigned to an individual label based on a 3×3 pixel neighbourhood. While UH thresholds are often based on model climatology using percentiles and are sensitive to grid point spacing and dynamical core employed, UH $\geq 75\ m^2{\cdot}s^{-2}$ (99.99th percentile in HIST) is the most common threshold used in operational research exploring supercells and captures relatively robust, cyclonic supercells (Ashley et al., 2023; Clark, Kain, et al., 2012; Gagne et al., 2017; Gallo et al., 2016; Gropp & Davenport, 2021; Molina et al., 2021; Sobash, Romine, et al., 2016; Sobash, Schwartz, et al., 2016). Once the UH tracks are compiled, a 10-km buffer is placed around each swath and checked for overlap between two consecutive hours to retain robust supercells (Burgess et al., 1982; Hocker & Basara, 2008; Wood et al., 1996). Here, three outcomes can arise: (1) there is no overlap, and the track is removed; (2) one overlap occurs, and the tracks are merged together or (3) more than one overlap occurs where the most similar region compared to the prior timestep is added to maintain track continuity. In the latter, the most similar region is determined by comparing the length, shape, area and intensity values of the surrounding regions to find the smallest difference to ensure that each track is unique and is not accounting for new initiation, splits, mergers and/or interruptions (Hungarian Method; Lakshmanan et al., 2013; Ashley et al., 2023). See Ashley et al. (2023) for a complete discussion of the tracking method and potential biases.

Two different UH thresholds are used to evaluate supercell candidates: $\geq 75\ m^2{\cdot}s^{-2}$ (herein UH75) and $\geq 60\ m^2{\cdot}s^{-2}$ (herein UH60). Using UH60 promotes a larger collection of supercell candidates that have long-lived (i.e., 2-h minimum criterion is retained) mesocyclones, yet may struggle to attain and/or maintain the more intense UH75 threshold for 2 h or more. Both thresholds are used as 'experiments' that are processed separately and while not a true superset, the UH60 experiment captures approximately twice the number of supercells, permitting a larger sample of candidates. The objective of two thresholds is to capture a spectrum of supercell candidates to ensure the UH75 method is not underrepresenting their hydroclimate contributions by solely examining very robust events.

2.4 | Accumulating supercell precipitation

WRF-BCC simulates precipitation using the Thompson et al. (2008) bulk water microphysics scheme, which resolves cloud water, rain, cloud ice, hail, snow and graupel. To explicitly obtain supercell precipitation within the WRF-BCC simulated output, UH tracks are used to provide the initial location and length of the robust mesocyclone, which, as discussed in the prior section, consists of any grid cell within the track that has a UH value of $\geq 75\ m^2{\cdot}s^{-2}$ ($\geq 60\ m^2{\cdot}s^{-2}$) for that hour. After sensitivity testing, a process known as watershed segmentation—an algorithm used for separating different objects within an image—is applied to separate, expand and capture a larger swath of a supercell's footprint by adding neighbouring grid cells, which have a UH value of $\geq 50\ m^2{\cdot}s^{-2}$ (herein UH50) surrounding the UH75 grid cells (Figure 1d–f). The UH60 experiment uses a watershed value of $\geq 40\ m^2{\cdot}s^{-2}$ (herein UH40), permitting consistency among the methods (i.e., UH40 is a direct comparative ratio to the UH75 and its watershed value of UH50). By including the surrounding UH50 (UH40) grid cells, the result is an extension of the UH75 (UH60) area, permitting an expansion of the original swath to better capture the storm's precipitating footprint (Figure 1a–f).

While the expanded swath is larger than before, further testing revealed that it does not sufficiently capture an entire storm's precipitating area in some cases. Therefore, an additional three-grid cell buffer (i.e., ∼10-km) is added to the outside UH50 (UH40) pixels that surround each UH75 (UH60) track (Figure 1d–f). This additional 10-km buffer was selected after buffer sensitivity analyses on 100 random event candidates, which revealed that 10 km was the best extension to obtain much, if not all, of the precipitation associated with a supercell's footprint, while removing extraneous precipitation from other nearby convective entities. Ultimately, a supercell's precipitation footprint is obtained by discarding any grid cell outside the buffer's area while retaining the precipitation data for the grid cells within the buffer (Figure 1g–i).

Visualization and testing hundreds of supercell candidates revealed that during the watershed process, exceedingly large UH swaths within a limited subset of mesoscale convective system (MCS) structures (e.g., particularly robust, fast-moving bowing segments) were created and did not adhere to the typical supercell definition. We did extensive testing on various minor axis length, major axis length, minor/major axis ratios and area size thresholds to mitigate the capturing of non-supercell candidates. The most effective solution included rules based on the 95th percentiles of the area and minor axis of the corresponding watershed buffer. Essentially, the algorithm removes any hourly watershed buffer greater than the 95th percentile for both the area and minor axis. However, if the watershed buffer is greater than the 95th percentile for area, but less than the 95th percentile for the minor axis, the candidate is retained (e.g., fast-moving supercells) and subsequently evaluated using the spatiotemporal thresholds previously discussed.

2.5 | Limitations

Due to the complexity of cataloguing supercells with current observational data—such as GridRad and MRMS, and the caveats associated with those data (e.g., radar beam height and beam filling; Fabry et al., 2017; Saltikoff et al., 2019)—this study uses simulated data (i.e., HIST) to build a climatology of supercell precipitation. While results obtained using observations are likely to differ (Ashley et al., 2023), the WRF-BCC horizontal grid spacing of 3.75 km is sufficient for the initiation and sustenance of deep, moist convection (Kendon et al., 2021; Weisman et al., 1997) and, thus, is a robust alternative for observed data. Recent work has suggested that finer grid spacing may be required to correctly account and solve for convective processes, especially when simulating supercells (Kendon et al., 2021; Prein et al., 2021). Additionally, CP-RCMs with >3-km grid spacing can have complications with boundary layer parametrization schemes (Schumacher, 2015), which may result in overall reduced supercell intensity (Fiori et al., 2010) and/or premature supercell weakening (Potvin & Flora, 2015; Verrelle et al., 2015). Nevertheless, while convective structures may be more realistic at higher resolutions, horizontal grid spacing of 3–4 km yields effective results at relatively smaller computational and time constraints (Bryan et al., 2003; Clark, Weiss, et al., 2012; Schwartz et al., 2009), especially considering this dataset spans three 15-year epochs and required significant computing and storage expenses.

Since the goal of this study is to quantify supercell precipitation output, this study is not biased to any supercell morphology (i.e., discrete or embedded); hence, all UH tracks that pass the aforementioned criteria are catalogued. However, tracking UH swaths using 2–5 km UH and a temporal threshold of 2 h retains primarily relatively long-lived, robust, cyclonic supercells. Moreover, left-moving (i.e., anticyclonic, with negative UH) supercells, and smaller, shallower, transient and/or weaker mesocyclones and/or mesovortices—especially those supercells associated with tropical cyclones (Morin & Parker, 2011) and quasi-linear convective systems (QLCSs; (Flournoy & Coniglio, 2019; Schenkman & Xue, 2016; Trapp & Weisman, 2003; Weisman & Trapp, 2003))—may not be captured (Ashley et al., 2019, 2023; Bunkers, 2002; Edwards et al., 2012; Smith et al., 2012; Sobash & Kain, 2017). Additional under-counting may arise from the nine-point smoothing performed on the UH values in simulation output (Ashley et al., 2023).

While most of the precipitation associated with a supercell's footprint is captured with the methods discussed, environmental and storm characteristics (e.g., mid-to-upper-level winds affecting precipitation ventilation and resulting in fast storm motions, deviant motion and storm splits/mergers) may result in the buffer missing a portion of the precipitation attributable to the supercell. Furthermore, since UH thresholds (i.e., UH75 and UH60) are used to segment, track and catalogue a supercell, only the mature phase of a robust supercell is captured. Initiation and dissipation phases of supercells, and their precipitation contributions, may not be captured due to lower UH values that typify these stages of an event's lifecycle.

3 | RESULTS

3.1 | Supercell climatology

The aforementioned methods produce the same mean annual UH75 supercell results as presented in Ashley

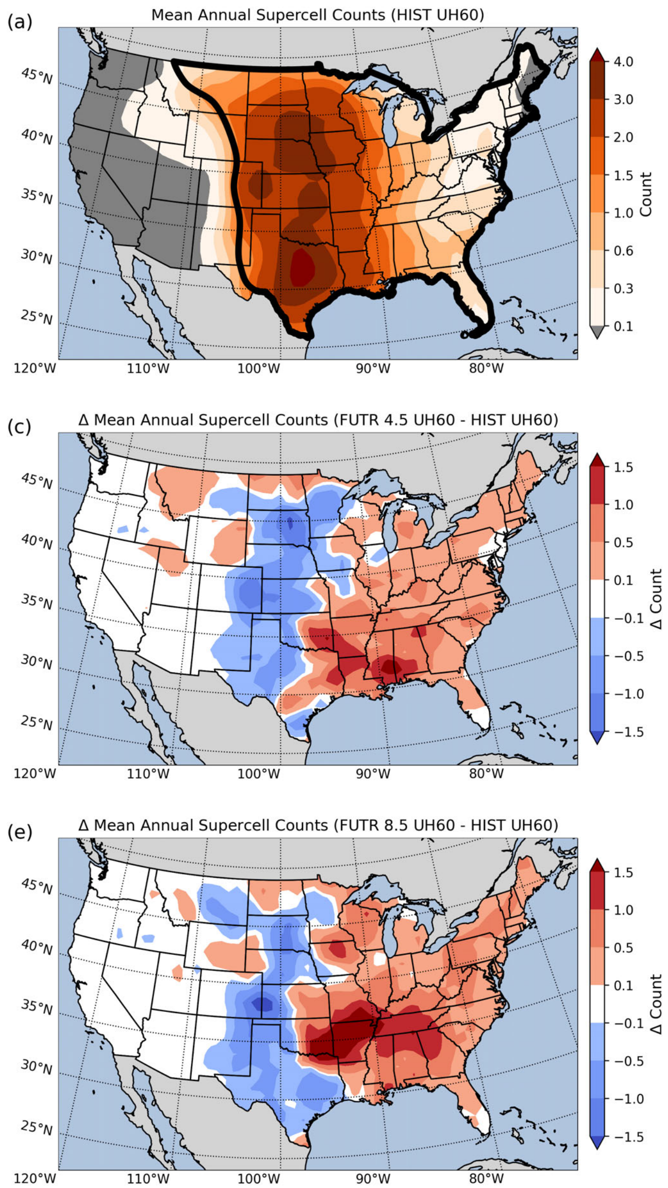

FIGURE 2 Mean annual HIST supercell track counts on an 80-km grid smoothed using a Gaussian kernel with $\sigma = 0.75$ for two UH thresholds: (a) HIST UH60 and (b) UH75. Corresponding deltas (i.e., FUTR–HIST) are presented in (c) FUTR 4.5 UH60, (d) FUTR 4.5 UH75, (e) FUTR 8.5 UH60 and (f) FUTR 8.5 UH75. (a) illustrates the ECONUS (east of Continental Divide; thick, solid outline) domain. See Figure 3c,e from Ashley et al. (2023) for statistical significance. [Colour figure can be viewed at wileyonlinelibrary.com]

et al. (2023) (Figure 2b). The climatology of UH60 supercells (Figure 2a) reveals a general step increase in frequency across regions that experience UH75 supercells. Overall, UH60 and UH75 supercells are most frequent across the central portions of the CONUS, with the greatest frequency stretching from Texas to the Dakotas and into the Midwest. Robust increases of annual supercell counts occur with UH60 and UH75 for both future climate epochs in comparison to the HIST (Figure 2c–f). Generally, increases in both UH60 and UH75 supercell counts are found across the eastern CONUS, roughly centred on and east of 95° W, with the greatest increases (upward of a doubling of annual supercell counts) expected across the Ozark Plateau, lower Mississippi and Ohio Valleys and Mid-South. Conversely, decreases in both UH60 and UH75 supercell counts are found across most of the Great Plains, stretching from Texas through the Dakotas. These results are generally supported by the observed changes in the current state of SCSs (i.e., tornado observations) in the CONUS, which show a decrease in SCS populations across the Great Plains and increases across portions of the Southeast and Midwest (e.g., Gensini et al., 2020; Gensini & Brooks, 2018). Presented changes in the mean annual

TABLE 1 Supercell precipitation contribution for the CONUS and ECONUS (east of the Continental Divide; see Figure 2a for domain).

CONUS domain	Precipitation contribution HIST (%)	Precipitation contribution FUTR 4.5 (%)	Precipitation contribution FUTR 8.5 (%)	Δ Contribution (%) HIST versus FUTR 4.5	Δ Contribution (%) HIST versus FUTR 8.5
UH60	1.04	1.25	1.44	20.73	**39.31**
UH75	0.60	0.74	0.85	22.99	**41.06**
ECONUS domain	**Precipitation contribution HIST (%)**	**Precipitation contribution FUTR 4.5 (%)**	**Precipitation contribution FUTR 8.5 (%)**	**Δ Contribution (%) HIST versus FUTR 4.5**	**Δ Contribution (%) HIST versus FUTR 8.5**
UH60	1.36	1.67	1.90	22.30	**39.46**
UH75	0.80	0.99	1.13	24.45	**41.17**

Note: Precipitation contribution is calculated by dividing the total annual supercell precipitation by the total annual precipitation for a specific domain. Deltas or changes, between the HIST and FUTR (4.5, 8.5) epochs under both UH thresholds are presented in the last two columns. Percent changes are all positive. Bold denotes a significant ($p < 0.05$; Mann–Whitney U test) difference between HIST and FUTR 8.5.

supercell counts are influenced by large increases in the south-central CONUS during spring and broad, but robust, decreases across most of the central CONUS during summer (Ashley et al., 2023).

3.2 | Supercell precipitation climatology

3.2.1 | Supercell precipitation contribution

Using HIST as a baseline climatology, long-lived, robust, cyclonic supercells or those classified as UH75, contribute 0.6% of the total annual precipitation to the CONUS hydroclimate, whereas, those classified as UH60, contribute 1.04% (Table 1). When restricted to the eastern CONUS (ECONUS)—where most supercells climatologically form (Figure 2a,b; Gensini & Ashley, 2011; Smith et al., 2012; Taszarek et al., 2020; Davenport, 2021; Ashley et al., 2023)—these percentage contributions increase to 0.8% and 1.36% for UH75 and UH60, respectively. These seemingly modest percentages are due to the relatively small size of supercells in comparison to other organized forms (i.e., MCSs, tropical cyclones) and the rarity of supercells compared to large populations of unorganized storms and stratiform events, which are the dominant modes of precipitation in the CONUS (e.g., Dai, 2001; Dai et al., 1999; Dai & Trenberth, 2004; Wallace, 1975). For example, the supercell's larger and more frequent organized counterpart, the MCS, contributes about 30% to the ECONUS hydroclimate (Haberlie & Ashley, 2019b). Supercell mean annual precipitation volume is about 35 km^3 for UH75 (55 km^3 UH60; Figure 3a,c), far less than MCSs, which yield 1398 km^3 on average annually (Haberlie & Ashley, 2019b). Henceforth, UH60 results will be provided parenthetically unless explicitly stated.

Spatially, the central CONUS receives the highest mean annual precipitation contribution from supercells, with percentage maxima over southeast South Dakota and south-central Texas. Each of these regions receive greater than 3% of their annual precipitation from UH75 supercells (>4% UH60; Figure 4c,d); these maxima correspond to regions with the greatest mean annual supercell populations (Figure 2a,b; Ashley et al., 2023). Outside of the central CONUS, supercells generally contribute <0.5% of the total mean annual precipitation due to the relatively uncommon occurrence of particularly long-lived, robust supercells in these parts of the country (Figure 2a,b).

Supercell precipitation contribution maximizes during the warm season—specifically April through July—with a seasonal maximum over south-central Texas at greater than 4% for UH75 supercells (>8% UH60; Figure S1c,d). Like the annual spatial pattern of supercell counts, the highest supercell precipitation contribution during the peak season of April through July is found across most of the central CONUS with decreasing contributions further west and east (Figure S1c,d). For the south-central CONUS, specifically, the supercell precipitation contribution is maximized during the spring with an average of 1.5% (>2.5%) across the region and a peak in southern Texas of greater than 7.5% (>10%). A poleward shift then occurs during summer where the north-central CONUS receives greater than 2.5% (>5%) of summer precipitation from supercells, with a peak precipitation contribution over South Dakota of greater than 7.5% (>10%; Figure S2c). The spatial pattern found in the warm season illustrates the relative importance of supercell precipitation to the agriculturally rich Wheat and Corn Belts, as well as those regions dependent on aquifers (e.g., Ogallala in the High Plains, Edwards in Texas, and Cambrian-Ordovician in the Midwest). Supercell

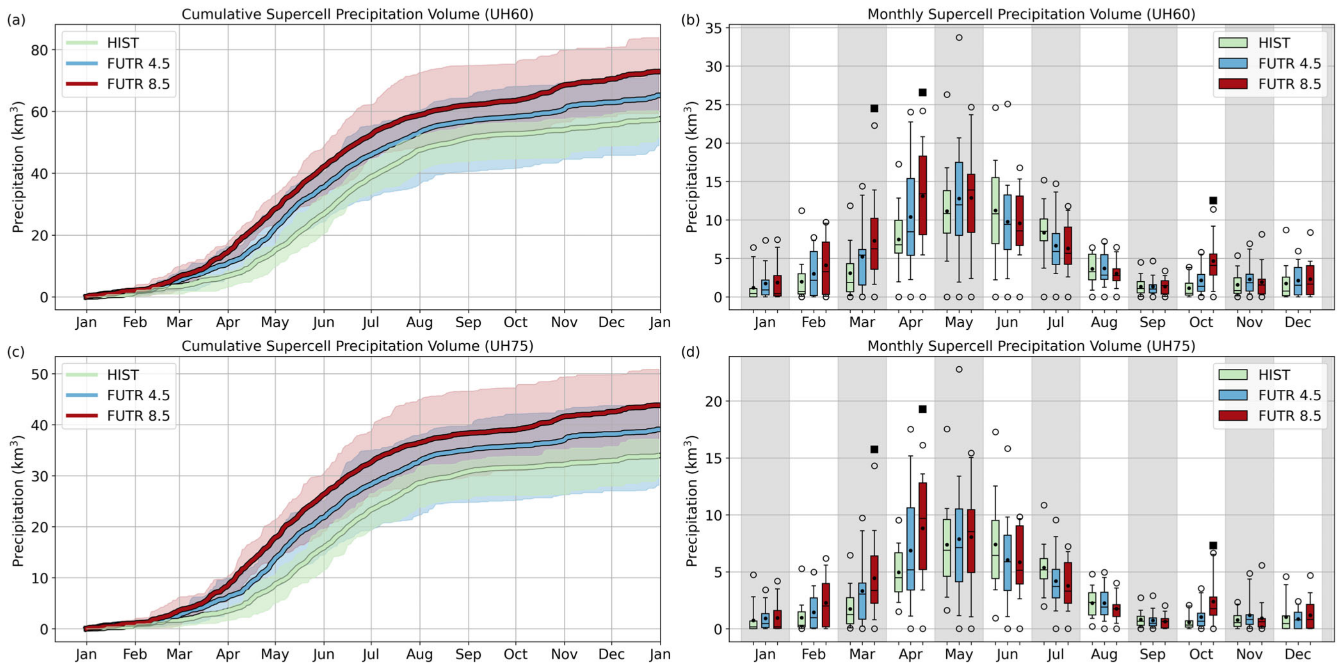

FIGURE 3 Annual cumulative frequency of volumetric supercell precipitation for HIST and FUTR (RCP 4.5, 8.5) periods for the ECONUS domain (see Figure 2a) under the (a) UH60 and (c) UH75 thresholds, as well as the monthly volumetric supercell precipitation (b,d) illustrated by Box-and-Whisker plots. In panels (a) and (c), means are denoted by thicker lines with the 25th and 75th percentiles provided in the corresponding epoch colour. For panels (b) and (d), means are denoted by black dots, medians by the black lines, the boxes represent the interquartile range, the Whiskers illustrate the 5th and 95th percentiles, and the clear circles denote outliers. A diamond (square) denotes a significant ($p < 0.05$; Mann–Whitney U test) difference between HIST and FUTR 4.5 (FUTR 8.5) epochs. [Colour figure can be viewed at wileyonlinelibrary.com]

precipitation contribution during fall is maximized across the central CONUS but is relatively low and highly variable (Figure S2d). During winter, supercell precipitation contribution is confined to the South, particularly along the Gulf Coast and in the Mid-South (Figure S2a).

Seasonal volumetric precipitation follows a similar pattern as seasonal supercell counts (Ashley et al., 2023) and is highest during spring and summer with seasonal means of 12 and 14 km^3, respectively, for UH75 supercells (21 and 25 km^3 UH60). Unsurprisingly, due to the seasonality of supercells, notably lower volumes are found during fall and winter (Figure 3b,d). Volumetrically, supercells contribute most to the ECONUS hydroclimate during April through July with upwards of 5 km^3 (>7 km^3) per month, with less than 3 km^3 (<5 km^3) per month from August through March (Figure 3b,d). Diurnally, cumulative volumetric supercell precipitation is maximized during the late evening to early night hours (23–04 UTC) and minimized during the morning (13–17 UTC), matching the frequency of supercell track counts (Figure 5a,b; Wallace, 1975; Ashley et al., 2023). Mean hourly supercell volumetric precipitation is maximized during the night to early afternoon hours resulting in a wide window for higher precipitating supercells (Figure S3a,c) when the public is particularly vulnerable to flash flooding (Ashley & Ashley, 2008).

3.2.2 | Per capita supercell analysis

Per capita (i.e., per supercell) central tendencies provide insight into the precipitation characteristics of a typical supercell, as well as the variability within the supercell population (Table 2). Viewing supercells as a source of extreme precipitation and subsequent flash flooding potential requires the assessment of precipitation rates and their duration over a single grid point. Typically, the higher the precipitation rate and the longer the duration of precipitation over a single point, the greater the potential for flash flooding (Doswell et al., 1996). On average, supercells produce a maximum precipitation rate of 44.0 mm·h^{-1} for UH75 supercells (41.9 mm·h^{-1} UH60; Table 2) over a mean area of 98.6 km^2·h^{-1} (95.7 km^2·h^{-1}); however, on average, these rates do not persist for more than a single hour. The mean areal extent of supercell-affiliated *extreme* precipitation rates

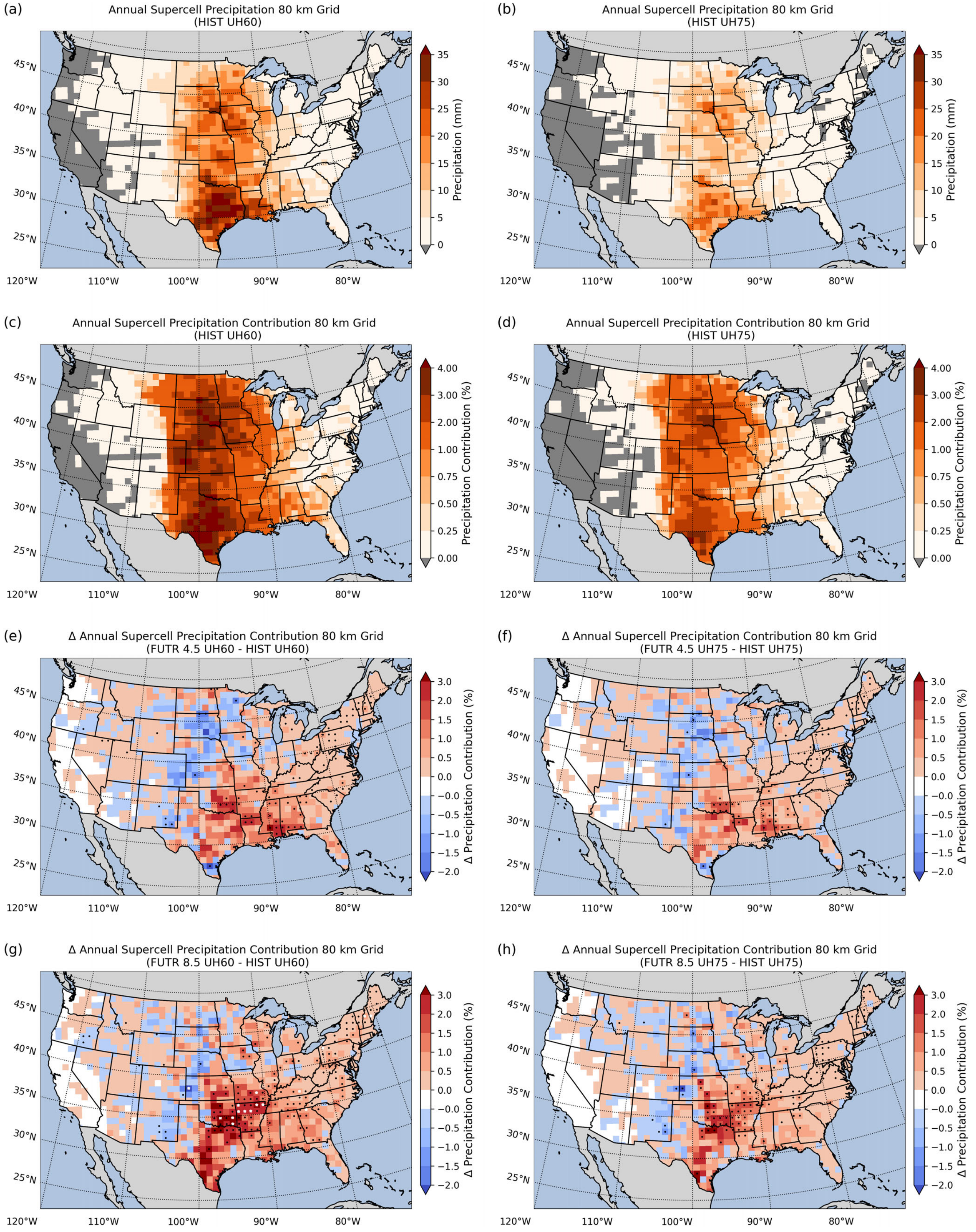

FIGURE 4 Legend on next page.

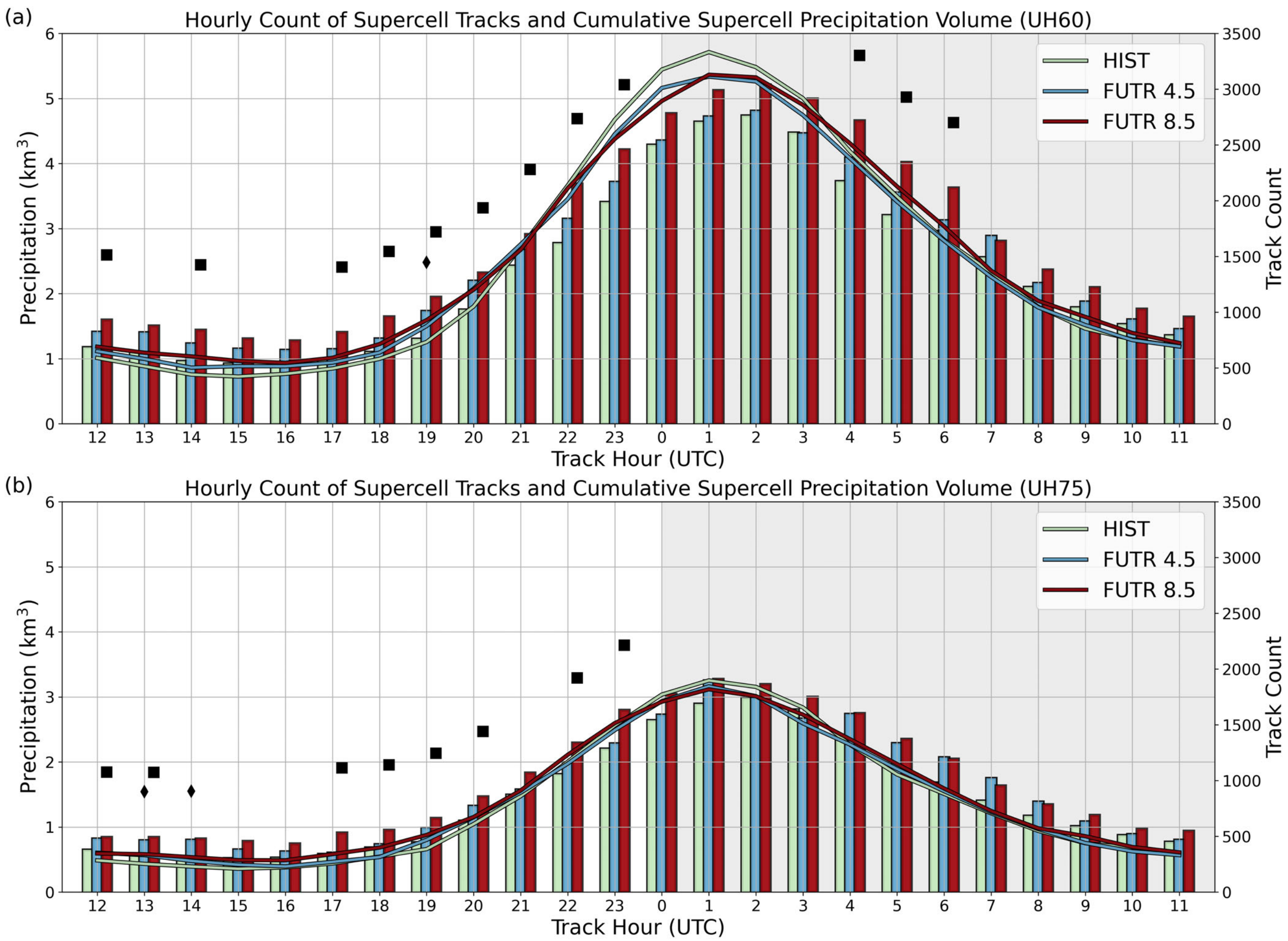

FIGURE 5 Total hourly supercell counts (lines) and volumetric supercell precipitation (bars) for the HIST and FUTR (RCP 4.5, 8.5) periods for the ECONUS domain (see Figure 2a) under the (a) UH60 and (b) UH75 thresholds. A diamond (square) denotes a significant ($p < 0.05$; Mann–Whitney U test) difference between HIST and FUTR 4.5 (FUTR 8.5) epochs. [Colour figure can be viewed at wileyonlinelibrary.com]

(e.g., ≥76.2 mm·h^{-1})—rates that require significantly less time to produce flash flood conditions—have a mean areal extent of 20.8 km^2 (24.7 km^2), which reveals how supercells can have extreme precipitation rates, but generally over very small footprints. These statistics are averaged over the entire HIST epoch, which does not provide context to tail end, or outlier, events that are most likely to produce conditions supportive of flash flooding (Figure S4; e.g., Smith et al., 2001, 2018).

3.2.3 | Supercell precipitation rates

Monthly mean supercell precipitation rates are maximized during the fall and winter (Figure 6a,c), likely influenced by the spatial distribution of supercells, which tend to exhibit greater coverage of higher precipitation rates during these seasons (discussed below). Conversely, the peak occurrence of monthly maximum precipitation rates from supercells occurs during the warm season,

FIGURE 4 Mean annual supercell precipitation totals (mm; (a) UH60, (b) UH75) and supercell precipitation contribution (% of total precipitation; (c) UH60, (d) UH75) on an 80-km grid for the HIST period. Corresponding deltas (i.e., FUTR–HIST) are presented in (e) (FUTR 4.5 UH60), (f) (FUTR 4.5 UH75), (g) (FUTR 8.5 UH60) and (h) (FUTR 8.5 UH75). Precipitation contribution is the sum of supercell-attributed precipitation divided by the total precipitation accumulation for each grid cell in the domain. Black stippling denotes a significant ($p < 0.05$; Mann–Whitney U test) difference between HIST and FUTR 4.5 or FUTR 8.5. White stippling denotes a significant ($p < 0.05$; Mann–Whitney U test) difference between HIST and FUTR 4.5 or FUTR 8.5 after a false discovery rate correction. [Colour figure can be viewed at wileyonlinelibrary.com]

TABLE 2 Measures of central tendency for annual per capita supercell precipitation metrics for the ECONUS domain (see Figure 2a) for UH75 and UH60 thresholds.

	HIST		FUTR 4.5		FUTR 8.5		Relative change (%) HIST versus FUTR 4.5		Relative change (%) HIST versus FUTR 8.5	
	UH60	UH75	UH60	UH75	UH60	UH75	UH60	UH75	UH60	UH75
Total volumetric supercell precipitation (km^3)										
Mean	0.06	0.06	0.07	0.07	0.07	0.08	11.88	12.54	20.44	20.70
Hourly volumetric supercell precipitation ($km^3 \cdot h^{-1}$)										
Mean	0.02	0.03	0.03	0.03	0.03	0.03	14.10	15.01	23.91	23.15
Supercell precipitation mean rate ($mm \cdot h^{-1}$)										
Mean	15.07	16.04	16.75	18.03	17.92	19.28	11.12	12.41	18.93	20.23
Supercell precipitation max rate ($mm \cdot h^{-1}$)										
Mean	41.92	44.01	44.58	47.26	46.80	49.47	6.32	7.39	11.64	12.40
Supercell precipitation footprint (km^2)										
Mean	3879.52	3885.71	3874.16	3875.88	3914.28	3906.76	−0.14*	−0.25*	0.9*	0.54*
Areal extent precipitation rate ≥25.40 $mm \cdot h^{-1}$										
Mean	822.51	913.38	973.38	1083.69	1067.19	1176.64	18.34	18.64	29.75	28.82
Areal extent precipitation rate ≥50.80 $mm \cdot h^{-1}$										
Mean	126.71	147.14	178.24	209.44	216.98	256.01	40.66	42.34	71.24	73.99
Areal extent precipitation rate ≥76.20 $mm \cdot h^{-1}$										
Mean	20.79	24.72	32.04	38.00	43.56	53.01	54.13	53.73	109.58	114.47
Areal extent precipitation rate ≥101.60 $mm \cdot h^{-1}$										
Mean	4.29	5.03	7.19	8.16	10.02	12.10	67.66	62.09	133.57	140.31
Areal extent precipitation rate ≥127.00 $mm \cdot h^{-1}$										
Mean	0.96	1.10	2.11	2.23	2.59	3.13	119.49	102.65*	170.13	184.45

Note: The four right columns include percentage changes in the mean for FUTR 4.5, 8.5 versus HIST. All values but those with * have a significant ($p < 0.05$; Mann–Whitney *U* test) difference between HIST and FUTR 4.5 or FUTR 8.5.

specifically from April through July (Figure 6b,d), corresponding to the period of highest supercell intensity throughout the year (Ashley et al., 2023) where a slight positive relationship (i.e., slope of 0.15 and correlation coefficient of 0.11) was found between the strength of the 2–5 km AGL UH and precipitation rates. A stronger relationship may exist with the strength of the low-level shear and subsequent low-level mesocyclone since both have been linked to enhanced precipitation production (Nielsen & Schumacher, 2018; Nielsen & Schumacher, 2020a; Nielsen & Schumacher, 2020b); however, this relationship cannot be examined since lower-layer UH data were not retained from the simulations. Additionally, a stronger supercell, as prescribed using UH, may not yield more precipitation depending on environmental characteristics (e.g., moisture quantity and depth; e.g., Grant and van den Heever, 2014; Morrison, 2017; Lasher-Trapp et al., 2021; Jo & Lasher-Trapp, 2022, 2023; Morrison et al., 2022; LeBel & Markowski, 2023); further study is needed to investigate environmental characteristics and the strength of various UH layers and magnitudes.

The southern CONUS experiences the most frequent extreme supercell-affiliated precipitation rates, particularly near the Gulf Coast (Figure 7a,b), likely tied to the maritime tropical airmass that frequently occurs in this region (i.e., higher precipitable water and deeper warm-rain formation; e.g., Kalkstein et al., 1998; Sheridan, 2002). A poleward expansion in extreme precipitation rates through the central CONUS is observed during the warm season and coincides with a region where low-level moisture advection from the Gulf of Mexico via the low-level jet is climatologically maximized (Bonner, 1968; Carbone & Tuttle, 2008; Lee et al., 2008; Nicolini et al., 1993; Pitchford & London, 1962; Pu & Dickinson, 2014; Weaver et al., 2012). The greatest cumulative area of supercell extreme precipitation rates occurs in April through July, which coincides with the highest cumulative supercell population and subsequent precipitation output (Figures 2, 3 and 8; Ashley et al., 2023).

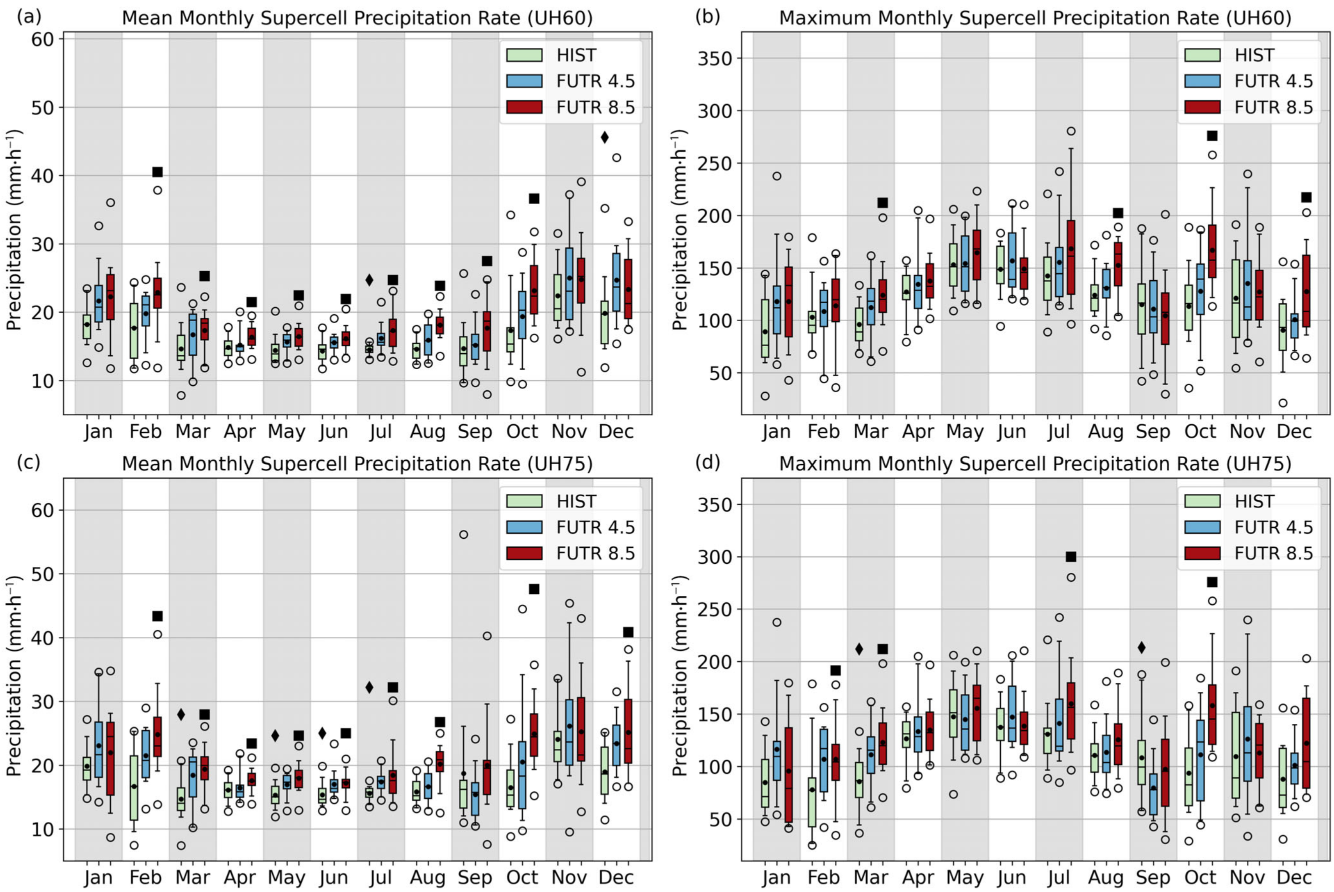

FIGURE 6 Monthly Box-and-Whisker plots illustrating mean ((a) UH60, (c) UH75) and maximum ((b) UH60, (d) UH75) precipitation rates for the HIST and FUTR (RCP 4.5, 8.5) periods for the ECONUS domain (see Figure 2a). Box-and-Whisker distributions and central tendencies as in Figure 3 are calculated by monthly mean and maximum precipitation rates averaged per supercell across each corresponding month. A diamond (square) denotes a significant ($p < 0.05$; Mann–Whitney U test) difference between HIST and FUTR 4.5 (FUTR8.5). [Colour figure can be viewed at wileyonlinelibrary.com]

3.3 | Projected changes in supercell precipitation

3.3.1 | Spatiotemporal changes in supercell precipitation contribution

With a likely increase in supercell counts by the end-of-the-21st-century (Figure 2c–f; Ashley et al., 2023), a corresponding increase in annual precipitation contribution from long-lived, robust, cyclonic supercells is expected (Table 1). Supercell precipitation contribution to the ECONUS hydroclimate is projected to increase by 24.5% for UH75 supercells (22.3% UH60) under the intermediate warming scenario (FUT4.5) and increase significantly ($p < 0.05$) by 41.2% (39.5%) under the pessimistic scenario (FUT8.5) (Table 1). Likewise, mean cumulative volumetric precipitation is projected to increase by 14.3% (18.2%) under FUTR 4.5 and by 22.9% (27.3%) under FUTR 8.5 (Figure 3a,c). Seasonal increases in supercell volumetric precipitation are expected for all seasons except summer, which decreases by 14.3% (13%) under FUTR 4.5 and 21.4% (26.1%) under FUTR 8.5. Indeed, projected declines in supercell precipitation volumetric contributions are most notable in June and July, possibly due to the increased capping and subsequent reduced event populations found during the mid-summer in the two climate change scenarios (Ashley et al., 2023; Haberlie et al., 2022). The most robust increase in supercell precipitation volumes, on the other hand, occurs during spring, with increases of 58.3% (46.3%) under FUTR 4.5 and 83.3% (70.7%) under FUTR 8.5.

The change in annual supercell precipitation contributions between the HIST and future epochs suggests a broad, yet variable, decrease across the Great Plains (e.g., greater than 0.5% (>1%) decrease) by the end-of-the-21st-century with increases generally centred on and east of 95° W (Figure 4e–h). The greatest projected increases in supercell precipitation contributions are statistically significant in the Ark-La-Tex and Ozark Plateau regions, which is similar to the pattern found for

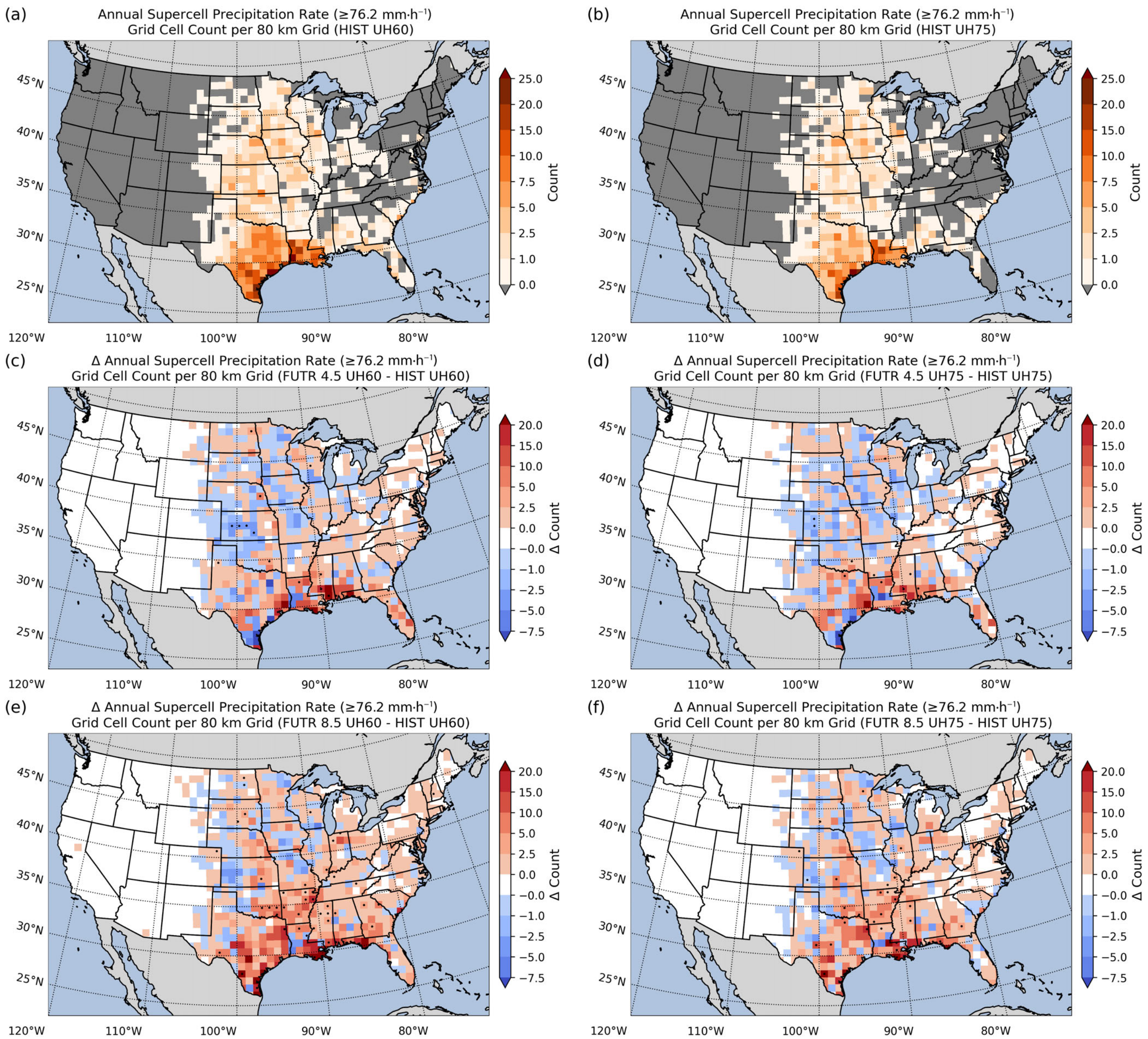

FIGURE 7 Mean annual cumulative supercell precipitation rates ≥76.2 mm·h^{-1} (≥3 in·h^{-1}) on an 80-km grid for HIST for (a) UH60 and (b) UH75 thresholds. Results are produced by taking all supercell grid cells ≥76.2 mm·h^{-1} across the domain and, thereafter, summed and averaged over the entire period for annual means. Corresponding deltas (i.e., FUTR–HIST) are presented in (c) (FUTR 4.5 UH60), (d) (FUTR 4.5 UH75), (e) (FUTR 8.5 UH60) and (f) (FUTR 8.5 UH75). Black stippling denotes a significant ($p < 0.05$; Mann–Whitney U test) difference between HIST and FUTR 4.5 or FUTR 8.5. [Colour figure can be viewed at wileyonlinelibrary.com]

supercell counts (Figures 2c–f and 4e–h; Ashley et al., 2023). Expected increases in precipitation contribution throughout these regions are greater than 1% (>1.5%) under FUTR 4.5 and greater than 1.5% (>2%) under FUTR 8.5 with varied significance after a false discovery rate correction. Broad increases in 21st-century supercell precipitation contributions include slight increases in both the western and eastern CONUS potentially owing to more supercells in the future in these regions (see discussion in Ashley et al. (2023)). Overall, narrow, but more impactful changes in supercell precipitation contributions appear in FUTR 8.5 with broader, yet muted, changes under FUTR 4.5 (Figure 4e–h).

Annual changes in supercell precipitation contribution are related to increases in supercell counts earlier in the year (Ashley et al., 2023), which are typically concentrated further south, thus increasing the supercell precipitation contribution in both the south and east compared to HIST. Annual changes in supercell precipitation contribution are affected by significant decreases during the summer months for much of the southern two-thirds of

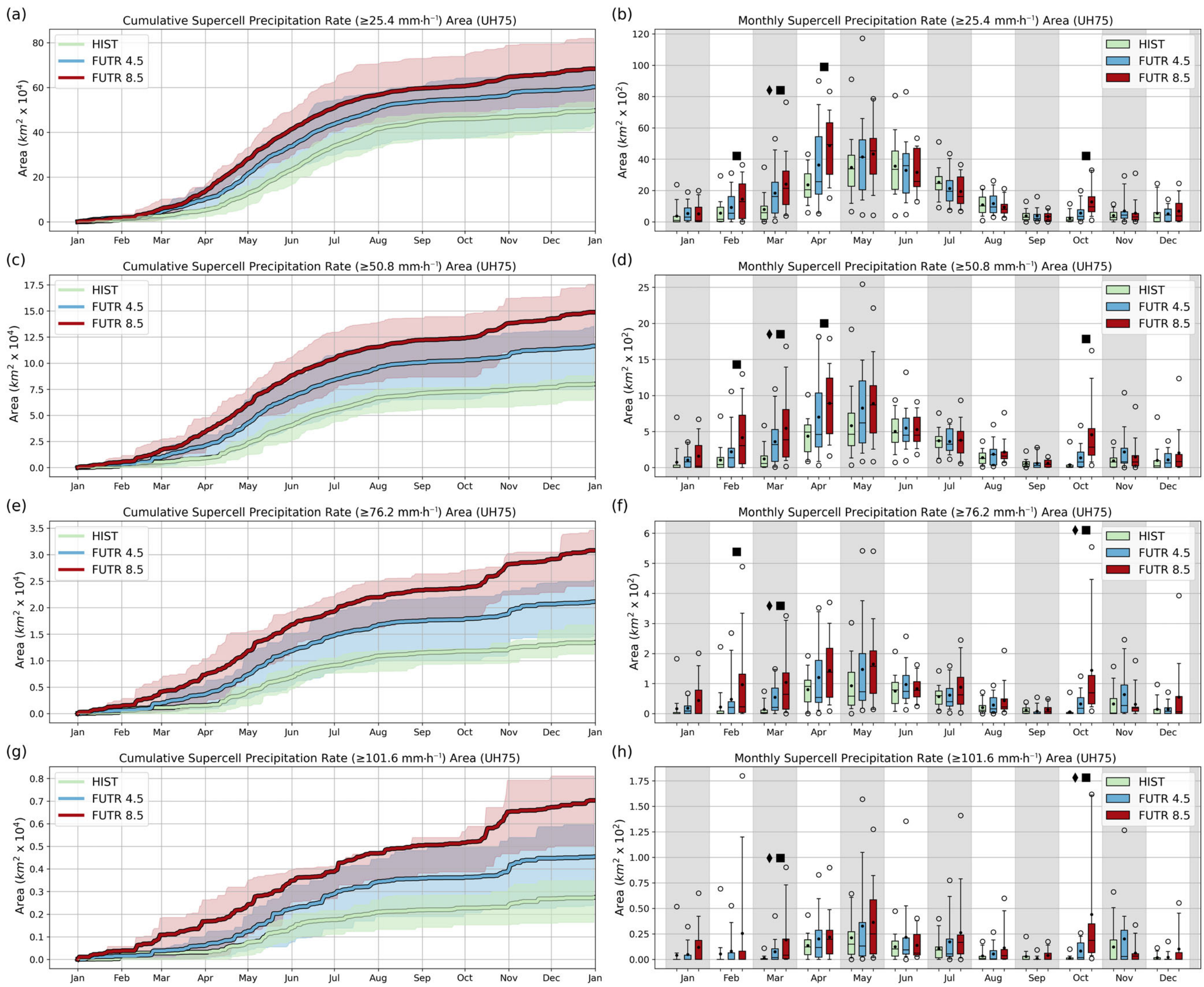

FIGURE 8 Annual cumulative area of various ((a) ≥25.4, (c) ≥50.8, (e) ≥76.2 and (g) ≥101.6 mm·h^{-1}; ((a) ≥1, (c) ≥2, (e) ≥3 and (g) ≥4 in·h^{-1}) supercell precipitation rates for the HIST and FUTR (RCP 4.5, 8.5) periods for the ECONUS domain (see Figure 2a) for (a) UH75 threshold, as well as the monthly cumulative area of corresponding precipitation rates ((b), (d), (f) and (h)) illustrated through Box-and-Whisker plots. Box-and-Whisker distributions and central tendencies as in Figure 3. A diamond (square) denotes a significant ($p < 0.05$; Mann–Whitney U test) difference between HIST and FUTR4.5 (FUTR8.5). Results are produced through the same methods as in Figure 1; however, each grid cell counted is converted to an area (i.e., km^2) to obtain a value of the total areal coverage of precipitation rates. [Colour figure can be viewed at wileyonlinelibrary.com]

the CONUS, with increases found roughly centred on and north of 42° N (Figure S2g,k). Mean monthly supercell precipitation contributions under FUTR 8.5 have broad increases during April through July compared to FUTR 4.5, particularly over the Great Plains, which is likely caused by a poleward increase in supercells under FUTR 8.5 (Figure S1e–h). This trend is further observed in seasonal changes during spring, which includes a poleward increase in supercell precipitation percentage contributions for FUTR 8.5, with a slight decrease in percentage contributions in the central CONUS for FUTR 4.5 (Figure S2f,j).

Diurnal changes in volumetric supercell precipitation show a net increase in the future for all hours with significant increases throughout most hours between 12 UTC and 23 UTC under FUTR 8.5 (Figure 5a,b). The overall pattern found in HIST holds for the future with both supercell counts and volumetric precipitation maximized during the evening and early night hours (23–05 UTC; Figure 5a,b). Diurnally, mean volumetric supercell precipitation increases notably in future epochs compared to HIST (Figure S3a,c), suggesting that future supercells will produce more precipitation under both intermediate and pessimistic climate change regimes. Furthermore, mean and maximum volumetric supercell precipitation increase robustly during the overnight and morning hours, consistent with an increasing trend for nocturnal supercells (Ashley et al., 2023). With the overnight hours characterized by higher vulnerability (Ashley & Ashley, 2008), this diurnal shift implies the public could be at a higher risk of potential flooding from supercells in the future.

3.3.2 | Changes in per capita supercell metrics

Significant ($p < 0.05$) changes in central tendencies of various supercell precipitation characteristics occur by the end-of-the-21st-century (Table 2). For example, mean total volumetric supercell precipitation is expected to increase by 12.5% for UH75 supercells (11.9% UH60) under the intermediate scenario and 20.7% (20.4%) under the pessimistic scenario. Likewise, mean hourly volumetric supercell precipitation is expected to increase by 15.0% (14.1%) for FUTR 4.5 and 23.2% (23.9%) for FUTR 8.5 (Table 2). The mean supercell precipitation hourly rate is projected to increase by 12.4% (11.1%) for FUTR 4.5 and 20.2% (18.9%) for FUTR 8.5, while the mean maximum hourly precipitation rate is projected to increase by 7.4% (6.3%) for FUTR 4.5 and 12.4% (11.6%) for FUTR 8.5 (Table 2). The cumulative areal extent of various supercell precipitation rates are projected to substantially increase by the end-of-the-21st-century (Table 2). The overall supercell precipitation footprint, however, is expected to decrease by 0.3% (0.1%) for FUTR 4.5 while increasing by only 0.5% (0.9%) for FUTR 8.5 (Table 2), suggesting that supercells will produce more precipitation in shorter durations and higher rates over roughly the same area, potentially leading to more runoff and a higher risk of flash floods.

Potential future risks of supercell-affiliated flooding are further amplified by an expected decrease in supercell translation speed. Specifically, mean annual supercell speeds are expected to decrease by 3.7% (1.9%) under FUTR 4.5 and decrease by 5.4% (2.7%) under FUTR 8.5 (not shown). The largest changes in supercell speeds are during June through September, which may decrease by 10% (24.8%) under FUTR 4.5 and decrease by 17.3% (33.5%) under FUTR 8.5, whereas, during the spring, supercell speeds may increase by 16.6% (18.3%) under FUTR 4.5 and increase by 6.0% (16.2%) under FUTR 8.5. The rest of the year (October–February), projected supercell speed changes are highly variable with no clear pattern (not shown). The expected changes in supercell precipitation characteristics further emphasize the impacts that supercells may have in the future as they become more efficient at producing precipitation over roughly the same areal coverage with, on average, a reduced translation speed.

3.3.3 | Spatiotemporal changes in supercell precipitation rates

Mean and maximum supercell precipitation rates increase annually in future epochs compared to HIST while maintaining similar seasonal distributions; mean precipitation rates peak during fall and winter, while maximum rates peak during spring and summer (Figure 6a–d). Mean supercell precipitation rates during the cool season are projected to increase by 29.4% (13.5%) under FUTR 4.5 and by 52.9% (24.3%) under FUTR 8.5 (Figure 6a,c). Maximum supercell precipitation rates during the warm season are also projected to increase by 4.4% (2.6%) under FUTR 4.5 and by 12% (13.2%) under FUTR 8.5 (Figure 6b,d). During the climatological peak months (March–August), monthly maximum supercell precipitation either increases or shows little change in the future, signifying an extended period of higher supercell precipitation totals and rates compared to HIST (Figure 6b,d). No clear shifts in the overall diurnal patterns emerge with hourly mean and maximum supercell precipitation rates projected to increase robustly for all hours of the day under both FUTR 4.5 and 8.5 (Figure S3b,d).

Spatially, changes in grid cell counts of supercell-affiliated extreme precipitation rates (e.g., $\geq$76.2 mm·h^{-1}) follow a pattern similar to the changes in supercell counts (Figure 2c–f; Ashley et al., 2023) and their precipitation (Figure 3). Specifically, changes in grid cell counts of extreme precipitation rates increase in the Southeast during all seasons except summer, where a broad decrease is projected throughout the central CONUS (e.g., Figure S5e–l). The largest changes in supercell-affiliated extreme precipitation rates occur during winter and spring with significant increases concentrated across eastern Texas and Oklahoma and a large portion of the Southeast (Figure S5e,f,i,j). During the summer, broad decreases in grid cell counts of supercell extreme precipitation rates are found over much of the CONUS, except for those states bordering Canada and in the Northeast (Figure S5g,k). This poleward increase is likely tied to the low-level jet, which is expected to transport richer moisture further north in the future (Rasmussen et al., 2020).

Annual cumulative area of various supercell precipitation rates are projected to increase considerably in the future (Figure 8). Specifically, the cumulative area of rates $\geq$101.8 mm·h^{-1} is projected to increase by 80% (116.7%) under FUTR 4.5 and 150% (250%) under FUTR

8.5. Monthly cumulative area of supercell extreme precipitation rates increase the most in future epochs during the cool and spring seasons (Figure 8b,d,f,h). Additionally, the expected decrease in supercell population during the summer months is offset by an increase in extreme precipitation rates per storm (Figure 8). These changes in areal coverage are likely tied to the spatial and temporal shifts in supercell counts, an increase in supportive environments for more vigorous supercells (Ashley et al., 2023) and the subsequent production of precipitation, and a change in supercell translation speeds.

4 | SUMMARY

This research presented a long-term climatology of supercell precipitation across the CONUS using output from a set of high-resolution, dynamically downscaled simulations. Spatial and temporal characteristics of supercells and their associated precipitation were evaluated along with an analysis of supercell precipitation rates for these extreme events. Results reveal that supercell precipitation is a relatively small (3%–6% in some regions), but not inconsequential, contributor to the ECONUS hydroclimate. Supercells provide critical precipitation to the Wheat and Corn Belts during the April through July period, which is a time when planting and maturation of crops is most prevalent. During the warm season, maximum supercell precipitation rates peak with a slight correlation with the peak in supercell intensity (Ashley et al., 2023). During the cool season, supercells become less frequent spatially and are concentrated further south where annual mean supercell precipitation rates maximize.

This research also investigated projected future changes in supercells and their associated precipitation, specifically in context of ACC by the end-of-the-21st-century. Two representations of supercells and their affiliated precipitation were provided for both intermediate and pessimistic warming scenarios. Projected changes of supercells in the future include an increase in supercell populations, precipitation contributions, precipitation totals and extreme precipitation rates. Specifically, projected end-of-21st-century changes include robust increases in supercell populations across portions of the south-central and Southeast regions with an annual decrease in supercell populations (Ashley et al., 2023) and affiliated precipitation contribution over most of the Great Plains. These spatial changes result from an earlier season in environments supportive for SCSs (Ashley et al., 2023) and projected increases in storm-suppressing CIN during the summer (Ashley et al., 2023; Hoogewind et al., 2017; Rasmussen et al., 2020).

Supercell precipitation rates generally increase in the future with most months either showing an increase in mean and maximum precipitation rates or little to no change in future climates. Per capita results show an increase in both total supercell precipitation and hourly totals with little change in supercell precipitation footprint size, signifying more intense precipitation cores in the future augmented by a decrease in translation speed. This intensification of supercell precipitation cores is further exacerbated through significant increases in the cumulative areal coverage of extreme supercell precipitation rates, which are projected to be two to five times the coverage found in HIST. These expected changes in precipitation characteristics are amplified by projected increases in both CAPE and precipitable water in future climates (Ashley et al., 2023; Haberlie et al., 2022; Held & Soden, 2006; Rasmussen et al., 2020; Trapp & Hoogewind, 2016; Trenberth, 1999; Trenberth et al., 2003). Specifically, the expected future increase in low-level water vapour will permit any updraft to ingest more water vapour and, thus, enhance both precipitation rates and total accumulations (Beatty et al., 2008; Doswell, 1998; Doswell et al., 1996; Hitchens & Brooks, 2013; Moller et al., 1990, 1994). Increases in CIN in future warm seasons may inhibit convective initiation and/or sustenance but may permit more vigorous updrafts potentially leading to an increase in precipitation production and rates when supercells do occur (Rasmussen et al., 2020; Trapp & Hoogewind, 2016).

Broadly, results from this study suggest stronger supercell precipitation events in the future. These changes may have implications for precipitation infiltration rates, runoff and flooding, particularly at local scales due to the relatively small footprint of most supercell swaths. Water-sensitive industries, private and public insurance markets and agricultural and public sectors will likely be increasingly affected by supercells and their enhanced precipitation rates in the future, especially in areas of the ECONUS such as the south-central Plains, Ozark Plateau and Mid-South (e.g., Gensini et al., 2020; Gensini & Brooks, 2018). Specifically, the expected changes in supercell precipitation contribution may have significant implications for agriculture as supercells may promote more impactful extreme precipitation rates, runoff and flooding during the planting season, with decreases in precipitation contribution during the summer months when crop growth is highly dependent on precipitation. The increased risk will likely coincide with increasing population and built-environment exposure, leading to increased runoff and flood potential and, ultimately, disaster (Collins et al., 2013; Hirabayashi et al., 2013; Koirala et al., 2014; Strader & Ashley, 2015).

While this study takes the first step in understanding the climatology of supercell precipitation and potential changes under ACC, further research is needed to generate a full understanding of supercell precipitation, both historically and in the future. Some avenues of future work include investigating regional differences in supercell precipitation, cataloguing training supercells for further analysis of flash flooding events, and analysing the most extreme events in more detail (e.g., Doswell, 1998; Smith et al., 2001, 2018). As computational capabilities advance, additional work employing convection-permitting simulations via dynamically downscaling is required. These simulations provide finer resolution—both spatial and temporally—information compared to GCMs and will continue to aid our understanding of the future of SCSs. Advancements in these simulations with an ensemble approach, such as using multiple GCM inputs, a variety of RCPs, different microphysical schemes, increased temporal and decreased spatial dimensions, use of multiple dynamical cores and a varying level of initial conditions and perturbations are needed to further our relatively limited understanding of future perils (Gensini, 2021). Future simulations, and the distillation of results from these datasets, will assist water-sensitive industries, governmental agencies, policymakers and the public in mitigating and building resilience in an era of rapid environmental and societal change.

AUTHOR CONTRIBUTIONS

Aaron W. Zeeb: Writing – original draft; investigation; conceptualization; methodology; visualization; validation. **Walker S. Ashley:** Writing – review and editing; project administration; supervision; methodology; conceptualization; resources. **Alex M. Haberlie:** Methodology; writing – review and editing; visualization; resources. **Vittorio A. Gensini:** Writing – review and editing; methodology; resources. **Allison C. Michaelis:** Methodology; writing – review and editing.

ACKNOWLEDGEMENT

This research was supported by the National Science Foundation Awards 1637225 and 1800582 and National Oceanic and Atmospheric Administration Award NA22OAR4690645. The authors acknowledge high-performance computing support from Cheyenne (doi:10.5065/D6RX99HX) provided by NCAR's Computational and Information Systems Laboratory, sponsored by the National Science Foundation. We also acknowledge and thank Dr. Michael Papka (ANL) for data storage and postprocessing assistance. This research used resources of the Argonne Leadership Computing Facility, which is a DOE Office of Science User Facility supported under Contract DE-AC02-06CH11357.

DATA AVAILABILITY STATEMENT

In the spirit of reproducibility, if an email request is made to the authors, we will make available data and materials necessary to interested researchers for duplication and verification of results herein. WRF-BCC simulation output is available in netCDF format and stored on NCAR and/or Argonne systems. We request that anyone interested in using the WRF-BCC output contact coauthor Gensini (vgensini@niu.edu) for information on how to access the data, including any collaboration.

ORCID

Aaron W. Zeeb https://orcid.org/0009-0005-4519-9329
Walker S. Ashley https://orcid.org/0000-0003-0816-3333
Alex M. Haberlie https://orcid.org/0000-0001-9172-4028
Vittorio A. Gensini https://orcid.org/0000-0001-6362-9197
Allison C. Michaelis https://orcid.org/0000-0002-0793-5779

REFERENCES

Allen, J.T. (2018) Climate change and severe thunderstorms. Oxford Research Encyclopedia of Climate Science, Climate Change and Severe Thunderstorms.

Allen, M.R. & Ingram, W.J. (2002) Constraints on future changes in climate and the hydrologic cycle. *Nature*, 419(6903), 228–232. Available from: https://doi.org/10.1038/nature01092

Ashley, S.T. & Ashley, W.S. (2008) Flood fatalities in the United States. *Journal of Applied Meteorology and Climatology*, 47(3), 805–818. Available from: https://doi.org/10.1175/2007JAMC1611.1

Ashley, W.S., Haberlie, A.M. & Gensini, V.A. (2023) The future of supercells in the United States. *Bulletin of the American Meteorological Society*, 104(1), E1–E21. Available from: https://doi.org/10.1175/BAMS-D-22-0027.1

Ashley, W.S., Haberlie, A.M. & Strohm, J. (2019) A climatology of quasi-linear convective systems and their hazards in the United States. *Weather and Forecasting*, 34(6), 1605–1631. Available from: https://doi.org/10.1175/WAF-D-19-0014.1

Attema, J.J., Loriaux, J.M. & Lenderink, G. (2014) Extreme precipitation response to climate perturbations in an atmospheric mesoscale model. *Environmental Research Letters*, 9(1), 014003. Available from: https://doi.org/10.1088/1748-9326/9/1/014003

Bacon, J. & Ortiz, J. (2023) "Once in every 1,000–2,000 years": storm swamps Fort Lauderdale with 25 inches of rain: updates. USA TODAY.

Ban, N., Schmidli, J. & Schär, C. (2015) Heavy precipitation in a changing climate: does short-term summer precipitation increase faster? *Geophysical Research Letters*, 42(4), 1165–1172. Available from: https://doi.org/10.1002/2014GL062588

Bao, J., Feng, J. & Wang, Y. (2015) Dynamical downscaling simulation and future projection of precipitation over China. *Journal of Geophysical Research: Atmospheres*, 120(16), 8227–8243. Available from: https://doi.org/10.1002/2015JD023275

Beatty, K., Rasmussen, E.N. & Straka, J.M. (2008) The supercell Spectrum. Part I: A Review of Research Related to Supercell Precipitation Morphology. 21.

Bonner, W.D. (1968) Climatology of the low level jet. *Monthly Weather Review*, 96(12), 833–850. Available from: https://doi.org/10.1175/1520-0493(1968)096<0833:COTLLJ>2.0.CO;2

Brooks, H.E. (2013) Severe thunderstorms and climate change. *Atmospheric Research*, 123, 129–138. Available from: https://doi.org/10.1016/j.atmosres.2012.04.002

Bruyère, C.L., Done, J.M., Holland, G.J. & Fredrick, S. (2014) Bias corrections of global models for regional climate simulations of high-impact weather. *Climate Dynamics*, 43(7), 1847–1856. Available from: https://doi.org/10.1007/s00382-013-2011-6

Bryan, G.H., Wyngaard, J.C. & Fritsch, J.M. (2003) Resolution requirements for the simulation of deep moist convection. *Monthly Weather Review*, 131(10), 2394–2416. Available from: https://doi.org/10.1175/1520-0493(2003)131<2394:RRFTSO>2.0.CO;2

Bunkers, M.J. (2002) Vertical wind shear associated with left-moving supercells. *Weather and Forecasting*, 17(4), 845–855. Available from: https://doi.org/10.1175/1520-0434(2002)017<0845:VWSAWL>2.0.CO;2

Bunkers, M.J. & Doswell, C.A. (2016) Comments on "Double impact: when both tornadoes and flash floods threaten the same place at the same time". *Weather and Forecasting*, 31(5), 1715–1721. Available from: https://doi.org/10.1175/WAF-D-16-0116.1

Burgess, D.W., Wood, V.T. & Brown, R.A. (1982) Mesoscyclone evolution statistics. San Antonio, TX.

Carbone, R.E. & Tuttle, J.D. (2008) Rainfall occurrence in the U.S. warm season: the diurnal cycle. *Journal of Climate*, 21(16), 4132–4146. Available from: https://doi.org/10.1175/2008JCLI2275.1

Chen, J. & Kumar, P. (2002) Role of terrestrial hydrologic memory in modulating ENSO impacts in North America. *Journal of Climate*, 15(24), 3569–3585. Available from: https://doi.org/10.1175/1520-0442(2003)015<3569:ROTHMI>2.0.CO;2

Christensen, J.H., Boberg, F., Christensen, O.B. & Lucas-Picher, P. (2008) On the need for bias correction of regional climate change projections of temperature and precipitation. *Geophysical Research Letters*, 35(20), 1–6. Available from: https://doi.org/10.1029/2008GL035694

Christian, J., Christian, K. & Basara, J.B. (2015) Drought and pluvial dipole events within the Great Plains of the United States. *Journal of Applied Meteorology and Climatology*, 54(9), 1886–1898. Available from: https://doi.org/10.1175/JAMC-D-15-0002.1

Clark, A.J., Kain, J.S., Marsh, P.T., Correia, J., Xue, M. & Kong, F. (2012) Forecasting tornado pathlengths using a three-dimensional object identification algorithm applied to convection-allowing forecasts. *Weather and Forecasting*, 27(5), 1090–1113. Available from: https://doi.org/10.1175/WAF-D-11-00147.1

Clark, A.J., Weiss, S.J., Kain, J.S., Jirak, I.L., Coniglio, M., Melick, C.J. et al. (2012) An overview of the 2010 hazardous weather testbed experimental forecast program spring experiment. *Bulletin of the American Meteorological Society*, 93(1), 55–74. Available from: https://doi.org/10.1175/BAMS-D-11-00040.1

Collins, M., Knutti, R., Arblaster, J., Dufresne, J.-L., Fichefet, T., Gao, X. et al. (2013) Long-term climate change: projections. *Commitments and Irreversibility*, 108, 1029–1136.

Dai, A. (2001) Global precipitation and thunderstorm frequencies. Part II: diurnal variations. *Journal of Climate*, 14(6), 1112–1128. Available from: https://doi.org/10.1175/1520-0442(2001)014<1112:GPATFP>2.0.CO;2

Dai, A., Giorgi, F. & Trenberth, K.E. (1999) Observed and model-simulated diurnal cycles of precipitation over the contiguous United States. *Journal of Geophysical Research: Atmospheres*, 104(D6), 6377–6402. Available from: https://doi.org/10.1029/98JD02720

Dai, A. & Trenberth, K.E. (2004) The diurnal cycle and its depiction in the community climate system model. *Journal of Climate*, 17(5), 930–951. Available from: https://doi.org/10.1175/1520-0442(2004)017<0930:TDCAID>2.0.CO;2

Dai, A., Zhao, T. & Chen, J. (2018) Climate change and drought: a precipitation and evaporation perspective. *Current Climate Change Reports*, 4(3), 301–312. Available from: https://doi.org/10.1007/s40641-018-0101-6

Davenport, C.E. (2021) Environmental evolution of long-lived supercell thunderstorms in the Great Plains. *Weather and Forecasting*, 36(6), 2187–2209. Available from: https://doi.org/10.1175/WAF-D-21-0042.1

Del Genio, A.D., Yao, M.-S. & Jonas, J. (2007) Will moist convection be stronger in a warmer climate? *Geophysical Research Letters*, 34(16) 1–5. Available from: https://doi.org/10.1029/2007GL030525

Diffenbaugh, N.S., Pal, J.S., Trapp, R.J. & Giorgi, F. (2005) Fine-scale processes regulate the response of extreme events to global climate change. *Proceedings of the National Academy of Sciences*, 102(44), 15774–15778. Available from: https://doi.org/10.1073/pnas.0506042102

Donat, M.G., Lowry, A.L., Alexander, L.V., O'Gorman, P.A. & Maher, N. (2016) More extreme precipitation in the world's dry and wet regions. *Nature Climate Change*, 6(5), 508–513. Available from: https://doi.org/10.1038/nclimate2941

Doswell, C.A. (1998) Seeing supercells as heavy rain producers. Preprints, 14th Conf. On hydrology, Dallas, *TX*. American Meteorology Society, 73–79.

Doswell, C.A., Brooks, H.E. & Maddox, R.A. (1996) Flash flood forecasting: an ingredients-based methodology. *Weather and Forecasting*, 11(4), 560–581. Available from: https://doi.org/10.1175/1520-0434(1996)011<0560:FFFAIB>2.0.CO;2

Duda, J.D. & Gallus, W.A. (2010) Spring and summer midwestern severe weather reports in supercells compared to other morphologies. *Weather and Forecasting*, 25(1), 190–206. Available from: https://doi.org/10.1175/2009WAF2222338.1

Ebrahimji, A., Sutton, J., Caldwell, T. & Gray, J. (2023) Fort Lauderdale airport to remain closed until Friday morning after the rainiest day in the city's history causes severe flooding. CNN.

Edwards, R., Dean, A.R., Thompson, R.L. & Smith, B.T. (2012) Convective modes for significant severe thunderstorms in the contiguous United States. Part III: tropical cyclone tornadoes. *Weather and Forecasting*, 27(6), 1507–1519. Available from: https://doi.org/10.1175/WAF-D-11-00117.1

Fabry, F., Meunier, V., Treserras, B.P., Cournoyer, A. & Nelson, B. (2017) On the climatological use of radar data mosaics: possibilities and challenges. *Bulletin of the American Meteorological Society*, 98(10), 2135–2148. Available from: https://doi.org/10.1175/BAMS-D-15-00256.1

Fiori, E., Parodi, A. & Siccardi, F. (2010) Turbulence closure parameterization and grid spacing effects in simulated supercell storms. *Journal of the Atmospheric Sciences*, 67(12), 3870–3890. Available from: https://doi.org/10.1175/2010JAS3359.1

Flournoy, M.D. & Coniglio, M.C. (2019) Origins of vorticity in a simulated tornadic mesovortex observed during PECAN on 6 July 2015. *Monthly Weather Review*, 147(1), 107–134. Available from: https://doi.org/10.1175/MWR-D-18-0221.1

Fowler, H.J., Lenderink, G., Prein, A.F., Westra, S., Allan, R.P., Ban, N. et al. (2021) Anthropogenic intensification of short-duration rainfall extremes. *Nature Reviews Earth & Environment*, 2(2), 107–122. Available from: https://doi.org/10.1038/s43017-020-00128-6

Gagne, D.J., McGovern, A., Haupt, S.E., Sobash, R.A., Williams, J.K. & Xue, M. (2017) Storm-based probabilistic hail forecasting with machine learning applied to convection-allowing ensembles. *Weather and Forecasting*, 32(5), 1819–1840. Available from: https://doi.org/10.1175/WAF-D-17-0010.1

Gallo, B.T., Clark, A.J. & Dembek, S.R. (2016) Forecasting tornadoes using convection-permitting ensembles. *Weather and Forecasting*, 31(1), 273–295. Available from: https://doi.org/10.1175/WAF-D-15-0134.1

Gensini, V.A. & Ashley, W.S. (2011) Climatology of potentially severe convective environments from the North American regional reanalysis. *E-Journal of Severe Storms Meteorology*, 6(8), 1–40. Available from: https://doi.org/10.55599/ejssm.v6i8.35

Gensini, V.A. & Brooks, H.E. (2018) Spatial trends in United States tornado frequency. *npj Climate and Atmospheric Science*, 1(1), 1–5. Available from: https://doi.org/10.1038/s41612-018-0048-2

Gensini, V.A., Haberlie, A.M. & Ashley, W.S. (2023) Convection-permitting simulations of historical and possible future climate over the contiguous United States. *Climate Dynamics*, 60(1), 109–126. Available from: https://doi.org/10.1007/s00382-022-06306-0

Gensini, V.A., Haberlie, A.M. & Marsh, P.T. (2020) Practically perfect Hindcasts of severe convective storms. *Bulletin of the American Meteorological Society*, 101(8), E1259–E1278. Available from: https://doi.org/10.1175/BAMS-D-19-0321.1

Gensini, V.A. & Mote, T.L. (2014) Estimations of hazardous convective weather in the United States using dynamical downscaling. *Journal of Climate*, 27(17), 6581–6589. Available from: https://doi.org/10.1175/JCLI-D-13-00777.1

Gensini, V.A. & Mote, T.L. (2015) Downscaled estimates of late 21st century severe weather from CCSM3. *Climatic Change*, 129(1), 307–321. Available from: https://doi.org/10.1007/s10584-014-1320-z

Gensini, V.(V.)A. (2021) Chapter 4—Severe convective storms in a changing climate. In: Fares, A. (Ed.) *Climate change and extreme events*. Amsterdam: Elsevier, pp. 39–56. Available from: https://doi.org/10.1016/B978-0-12-822700-8.00007-X

Giordano, L.A. & Fritsch, J.M. (1991) Strong tornadoes and flash-flood-producing rainstorms during the warm season in the mid-Atlantic region. *Weather and Forecasting*, 6(4), 437–455. Available from: https://doi.org/10.1175/1520-0434(1991)006<0437:STAFFP>2.0.CO;2

Giorgi, F. & Mearns, L.O. (1999) Introduction to special section: regional climate modeling revisited. *Journal of Geophysical Research: Atmospheres*, 104(D6), 6335–6352. Available from: https://doi.org/10.1029/98JD02072

Grant, L.D. & van den Heever, S.C. (2014) Microphysical and dynamical characteristics of low-precipitation and classic supercells. *Journal of the Atmospheric Sciences*, 71(7), 2604–2624. Available from: https://doi.org/10.1175/JAS-D-13-0261.1

Gropp, M.E. & Davenport, C.E. (2021) Python-based supercell tracking for coarse temporal and spatial resolution numerical model simulations. *Journal of Atmospheric and Oceanic Technology*, 38(9), 1551–1559. Available from: https://doi.org/10.1175/JTECH-D-20-0122.1

Gutowski, W.J., Hegerl, G., Holland, J.G., Knutson, T.R., Mearns, L.O., Stouffer, R.J. et al. (2008) Causes of observed changes in extreme projections of future changes. *Weather and Climate Extremes in a Changing Climate CCSP Synthesis and Assessment Product*, 3(3), 81–116.

Haberlie, A.M. & Ashley, W.S. (2019a) Climatological representation of mesoscale convective systems in a dynamically downscaled climate simulation. *International Journal of Climatology*, 39(2), 1144–1153. Available from: https://doi.org/10.1002/joc.5880

Haberlie, A.M. & Ashley, W.S. (2019b) A radar-based climatology of mesoscale convective systems in the United States. *Journal of Climate*, 32(5), 1591–1606. Available from: https://doi.org/10.1175/JCLI-D-18-0559.1

Haberlie, A.M., Ashley, W.S., Battisto, C.M. & Gensini, V.A. (2022) Thunderstorm activity under intermediate and extreme climate change scenarios. *Geophysical Research Letters*, 49(14), e2022GL098779. Available from: https://doi.org/10.1029/2022GL098779

Held, I.M. & Soden, B.J. (2006) Robust responses of the hydrological cycle to global warming. *Journal of Climate*, 19(21), 5686–5699. Available from: https://doi.org/10.1175/JCLI3990.1

Hirabayashi, Y., Mahendran, R., Koirala, S., Konoshima, L., Yamazaki, D., Watanabe, S. et al. (2013) Global flood risk under climate change. *Nature Climate Change*, 3(9), 816–821. Available from: https://doi.org/10.1038/nclimate1911

Hitchens, N.M. & Brooks, H.E. (2013) Preliminary investigation of the contribution of supercell thunderstorms to the climatology of heavy and extreme precipitation in the United States. *Atmospheric Research*, 123, 206–210. Available from: https://doi.org/10.1016/j.atmosres.2012.06.023

Hocker, J.E. & Basara, J.B. (2008) A geographic information systems–based analysis of supercells across Oklahoma from 1994 to 2003. *Journal of Applied Meteorology and Climatology*, 47(5), 1518–1538. Available from: https://doi.org/10.1175/2007JAMC1673.1

Hoogewind, K.A., Baldwin, M.E. & Trapp, R.J. (2017) The impact of climate change on hazardous convective weather in the United States: insight from high-resolution dynamical downscaling. *Journal of Climate*, 30(24), 10081–10100. Available from: https://doi.org/10.1175/JCLI-D-16-0885.1

Hurrell, J., Holland, M.M., Gent, P.R., Ghan, S.J., Kay, J., Kushner, P. et al. (2013) The community earth system model: A framework for collaborative research. *Bulletin of the American Meteorological Society*, 94(9), 1339–1360. Available from: https://doi.org/10.1175/BAMS-D-12-00121

Ines, A.V.M. & Hansen, J.W. (2006) Bias correction of daily GCM rainfall for crop simulation studies. *Agricultural and Forest Meteorology*, 138(1–4), 44–53. Available from: https://doi.org/10.1016/j.agrformet.2006.03.009

IPCC, 2021: Climate Change 2021: The Physical Science Basis. Contribution of Working Group I to the Sixth Assessment Report of the Intergovernmental Panel on Climate Change[Masson-Delmotte, V., P. Zhai, A. Pirani, S.L. Connors, C. Péan, S. Berger, N. Caud, Y. Chen, L. Goldfarb, M.I. Gomis, M. Huang, K. Leitzell, E. Lonnoy, J.B.R. Matthews, T.K. Maycock, T. Waterfield, O. Yelekçi, R. Yu, and B. Zhou (eds.)]. Cambridge University Press, Cambridge, United Kingdom and New York, NY, USA, In press, https://doi.org/10.1017/9781009157896

IPCC, 2014: Climate Change 2014: Synthesis Report. Contribution of Working Groups I, II and III to the Fifth Assessment Report of the Intergovernmental Panel on Climate Change [Core Writing Team, R.K. Pachauri and L.A. Meyer (eds.)]. IPCC, Geneva, Switzerland, 151 pp.

Ives, M. & Hauser, C. (2023) Fort Lauderdale is drenched with up to two feet of rain, shutting its airport. *The New York Times*, 13 April.

Jo, E. & Lasher-Trapp, S. (2022) Entrainment in a simulated supercell thunderstorm. Part II: the influence of vertical wind shear and general effects upon precipitation. *Journal of the Atmospheric Sciences*, 79(5), 1429–1443. Available from: https://doi.org/10.1175/JAS-D-21-0289.1

Jo, E. & Lasher-Trapp, S. (2023) Entrainment in a simulated supercell thunderstorm. Part III: the influence of decreased environmental humidity and general effects upon precipitation efficiency. *Journal of the Atmospheric Sciences*, 80(4), 1107–1122. Available from: https://doi.org/10.1175/JAS-D-22-0168.1

Kain, J.S., Weiss, S.J., Bright, D.R., Baldwin, M.E., Levit, J.J., Carbin, G.W. et al. (2008) Some practical considerations regarding horizontal resolution in the first generation of operational convection-allowing NWP. *Weather and Forecasting*, 23(5), 931–952. Available from: https://doi.org/10.1175/WAF2007106.1

Kalkstein, L.S., Sheridan, S.C. & Graybeal, D.Y. (1998) A determination of character and frequency changes in air masses using a spatial synoptic classification. *International Journal of Climatology: A Journal of the Royal Meteorological Society*, 18(11), 1223–1236.

Karl, T.R. & Trenberth, K.E. (2003) Modern global climate change. *Science*, 302(5651), 1719–1723. Available from: https://doi.org/10.1126/science.1090228

Kendon, E.J., Prein, A.F., Senior, C.A. & Stirling, A. (2021) Challenges and outlook for convection-permitting climate modelling. *Philosophical Transactions of the Royal Society A: Mathematical, Physical and Engineering Sciences*, 379(2195), 20190547. Available from: https://doi.org/10.1098/rsta.2019.0547

Kendon, E.J., Roberts, N.M., Fowler, H.J., Roberts, M.J., Chan, S.C. & Senior, C.A. (2014) Heavier summer downpours with climate change revealed by weather forecast resolution model. *Nature Climate Change*, 4(7), 570–576. Available from: https://doi.org/10.1038/nclimate2258

Kendon, E.J., Roberts, N.M., Senior, C.A. & Roberts, M.J. (2012) Realism of rainfall in a very high-resolution regional climate model. *Journal of Climate*, 25(17), 5791–5806. Available from: https://doi.org/10.1175/JCLI-D-11-00562.1

Kirtman, B., Power, S.B., Adedoyin, A.J., Boer, G.J., Bojariu, R., Camilloni, I. et al. (2013) Chapter 11—Near-term climate change: projections and predictability. In: *IPCC*. Cambridge: Cambridge University Press.

Koirala, S., Hirabayashi, Y., Mahendran, R. & Kanae, S. (2014) Global assessment of agreement among streamflow projections using CMIP5 model outputs. *Environmental Research Letters*, 9(6), 064017. Available from: https://doi.org/10.1088/1748-9326/9/6/064017

Kunkel, K.E., Karl, T.R., Brooks, H., Kossin, J., Lawrimore, J.H., Arndt, D. et al. (2013) Monitoring and understanding trends in extreme storms: state of knowledge. *Bulletin of the American Meteorological Society*, 94(4), 499–514. Available from: https://doi.org/10.1175/BAMS-D-11-00262.1

Lakshmanan, V., Miller, M. & Smith, T. (2013) Quality control of accumulated fields by applying spatial and temporal constraints. *Journal of Atmospheric and Oceanic Technology*, 30(4), 745–758. Available from: https://doi.org/10.1175/JTECH-D-12-00128.1

Lasher-Trapp, S., Jo, E., Allen, L.R., Engelsen, B.N. & Trapp, R.J. (2021) Entrainment in a simulated supercell thunderstorm. Part I: the evolution of different entrainment mechanisms and their dilutive effects. *Journal of the Atmospheric Sciences*, 78(9), 2725–2740. Available from: https://doi.org/10.1175/JAS-D-20-0223.1

LeBel, L.J. & Markowski, P.M. (2023) An analysis of the impact of vertical wind shear on convection initiation using Large-Eddy simulations: importance of wake entrainment. *Monthly Weather Review*, 151(7), 1667–1688. Available from: https://doi.org/10.1175/MWR-D-22-0176.1

Lee, M.-I., Schubert, S.D., Suarez, M.J., Schemm, J.-K.E., Pan, H.-L., Han, J. et al. (2008) Role of convection triggers in the simulation of the diurnal cycle of precipitation over the United States Great Plains in a general circulation model. *Journal of Geophysical Research: Atmospheres*, 113(D2). Available from: https://doi.org/10.1029/2007JD008984

Liu, C., Ikeda, K., Rasmussen, R., Barlage, M., Newman, A.J., Prein, A.F. et al. (2017) Continental-scale convection-permitting modeling of the current and future climate of North America. *Climate Dynamics*, 49(1–2), 71–95. Available from: https://doi.org/10.1007/s00382-016-3327-9

Markowski, P.M. & Richardson, Y. (2010) *Mesoscale meteorology in midlatitudes*. Hoboken, NJ: Wiley-Blackwell, p. 432. Available from: https://doi.org/10.1002/9780470682104

Meehl, G.A., Arblaster, J.M. & Tebaldi, C. (2005) Understanding future patterns of increased precipitation intensity in climate model simulations. *Geophysical Research Letters*, 32(18), 1–4. Available from: https://doi.org/10.1029/2005GL023680

Miguez-Macho, G., Stenchikov, G.L. & Robock, A. (2004) Spectral nudging to eliminate the effects of domain position and geometry in regional climate model simulations. *Journal of Geophysical Research: Atmospheres*, 109(D13), 1–14. Available from: https://doi.org/10.1029/2003JD004495

Min, S.-K., Zhang, X., Zwiers, F.W., Friederichs, P. & Hense, A. (2009) Signal detectability in extreme precipitation changes assessed from twentieth century climate simulations. *Climate Dynamics*, 32(1), 95–111. Available from: https://doi.org/10.1007/s00382-008-0376-8

Min, S.-K., Zhang, X., Zwiers, F.W. & Hegerl, G.C. (2011) Human contribution to more-intense precipitation extremes. *Nature*, 470(7334), 378–381. Available from: https://doi.org/10.1038/nature09763

Molina, M.J., Gagne, D.J. & Prein, A.F. (2021) A benchmark to test generalization capabilities of deep learning methods to classify severe convective storms in a changing climate. *Earth and Space Science*, 8(9), e2020EA001490. Available from: https://doi.org/10.1029/2020EA001490

Moller, A.R., Doswell, C.A., Foster, M.P. & Woodall, G.R. (1994) The operational recognition of supercell thunderstorm environments and storm structures. *Weather and Forecasting*, 9(3), 327–347. Available from: https://doi.org/10.1175/1520-0434(1994)009<0327:TOROST>2.0.CO;2

Moller, A.R., Doswell, C.A. & Przybylinski, R. (1990) High-precipitation supercells: A conceptual model and documentation. Preprints, 16th Conference on Severe Local Storms, pp. 52–57.

Morin, M.J. & Parker, M.D. (2011) A numerical investigation of supercells in landfalling tropical cyclones. *Geophysical Research Letters*, 38(10) 1–7. Available from: https://doi.org/10.1029/2011GL047448

Morrison, H. (2017) An analytic description of the structure and evolution of growing deep cumulus updrafts. *Journal of the Atmospheric Sciences*, 74(3), 809–834. Available from: https://doi.org/10.1175/JAS-D-16-0234.1

Morrison, H., Peters, J.M., Chandrakar, K.K. & Sherwood, S.C. (2022) Influences of environmental relative humidity and horizontal scale of subcloud ascent on deep convective initiation. *Journal of the Atmospheric Sciences*, 79(2), 337–359. Available from: https://doi.org/10.1175/JAS-D-21-0056.1

Moss, R. H., Edmonds, J. A., Hibbard, K. A., Manning, M. R., Rose, S. K., van Vuuren, D. P., Carter, T. R., Emori, S., Kainuma, M., Kram, T., Meehl, G. A., Mitchell, J. F. B., Nakicenovic, N., Riahi, K., Smith, S. J., Stouffer, R. J., Thomson, A. M., Weyant, J. P., & Wilbanks, T. J. (2010). The next generation of scenarios for climate change research and assessment. *Nature*, 463(7282), 747–756. https://doi.org/10.1038/nature08823

Muller, C.J., O'Gorman, P.A. & Back, L.E. (2011) Intensification of precipitation extremes with warming in a cloud-resolving model. *Journal of Climate*, 24(11), 2784–2800. Available from: https://doi.org/10.1175/2011JCLI3876.1

Naylor, J., Gilmore, M.S., Thompson, R.L., Edwards, R. & Wilhelmson, R.B. (2012) Comparison of objective supercell identification techniques using an idealized cloud model. *Monthly Weather Review*, 140(7), 2090–2102. Available from: https://doi.org/10.1175/MWR-D-11-00209.1

Nicolini, M., Waldron, K.M. & Paegle, J. (1993) Diurnal oscillations of low-level jets, vertical motion, and precipitation: A model case study. *Monthly Weather Review*, 121(9), 2588–2610. Available from: https://doi.org/10.1175/1520-0493(1993)121<2588:DOOLLJ>2.0.CO;2

Nielsen, E.R., Herman, G.R., Tournay, R.C., Peters, J.M. & Schumacher, R.S. (2015) Double impact: when both tornadoes and flash floods threaten the same place at the same time. *Weather and Forecasting*, 30(6), 1673–1693. Available from: https://doi.org/10.1175/WAF-D-15-0084.1

Nielsen, E.R. & Schumacher, R.S. (2018) Dynamical insights into extreme short-term precipitation associated with supercells and mesovortices. *Journal of the Atmospheric Sciences*, 75(9), 2983–3009. Available from: https://doi.org/10.1175/JAS-D-17-0385.1

Nielsen, E.R. & Schumacher, R.S. (2020a) Dynamical mechanisms supporting extreme rainfall accumulations in the Houston "tax day" 2016 flood. *Monthly Weather Review*, 148(1), 83–109. Available from: https://doi.org/10.1175/MWR-D-19-0206.1

Nielsen, E.R. & Schumacher, R.S. (2020b) Observations of extreme short-term precipitation associated with supercells and mesovortices. *Monthly Weather Review*, 148(1), 159–182. Available from: https://doi.org/10.1175/MWR-D-19-0146.1

NOAA. (1995) National disaster survey report: The Fort Worth–Dallas hailstorm and flash flood of May 5, 1995. National Weather Service, Silver Spring, MD, 39 pp.

O'Gorman, P.A. & Schneider, T. (2009) The physical basis for increases in precipitation extremes in simulations of 21st-century climate change. *Proceedings of the National Academy of Sciences*, 106(35), 14773–14777. Available from: https://doi.org/10.1073/pnas.0907610106

Pall, P., Allen, M.R. & Stone, D.A. (2007) Testing the Clausius–Clapeyron constraint on changes in extreme precipitation under CO_2 warming. *Climate Dynamics*, 28(4), 351–363. Available from: https://doi.org/10.1007/s00382-006-0180-2

Peters, J.M., Morrison, H., Nowotarski, C.J., Mulholland, J.P. & Thompson, R.L. (2020) A formula for the maximum vertical velocity in supercell updrafts. *Journal of the Atmospheric Sciences*, 77(11), 3747–3757. Available from: https://doi.org/10.1175/JAS-D-20-0103.1

Peters, J.M., Mulholland, J.P. & Chavas, D.R. (2022) Generalized lapse rate formulas for use in entraining CAPE calculations. *Journal of the Atmospheric Sciences*, 79(3), 815–836. Available from: https://doi.org/10.1175/JAS-D-21-0118.1

Peters, J.M., Nowotarski, C.J. & Morrison, H. (2019) The role of vertical wind shear in modulating maximum supercell updraft velocities. *Journal of the Atmospheric Sciences*, 76(10), 3169–3189. Available from: https://doi.org/10.1175/JAS-D-19-0096.1

Peters, J.M., Nowotarski, C.J. & Mullendore, G.L. (2020) Are supercells resistant to entrainment because of their rotation? *Journal of the Atmospheric Sciences*, 77(4), 1475–1495. Available from: https://doi.org/10.1175/JAS-D-19-0316.1

Pilguj, N., Taszarek, M., Allen, J.T. & Hoogewind, K.A. (2022) Are trends in convective parameters over the United States and Europe consistent between reanalyses and observations? *Journal of Climate*, 35(12), 3605–3626. Available from: https://doi.org/10.1175/JCLI-D-21-0135.1

Pitchford, K.L. & London, J. (1962) The low-level jet as related to nocturnal thunderstorms over Midwest United States. *Journal of Applied Meteorology and Climatology*, 1(1), 43–47. Available from: https://doi.org/10.1175/1520-0450(1962)001<0043:TLLJAR>2.0.CO;2

Potvin, C.K. & Flora, M.L. (2015) Sensitivity of idealized supercell simulations to horizontal grid spacing: implications for warn-on-forecast. *Monthly Weather Review*, 143(8), 2998–3024. Available from: https://doi.org/10.1175/MWR-D-14-00416.1

Prein, A.F., Liu, C., Ikeda, K., Trier, S.B., Rasmussen, R.M., Holland, G.J. et al. (2017) Increased rainfall volume from future convective storms in the US. *Nature Climate Change*, 7(12), 880–884. Available from: https://doi.org/10.1038/s41558-017-0007-7

Prein, A.F., Rasmussen, R.M., Ikeda, K., Liu, C., Clark, M.P. & Holland, G.J. (2017) The future intensification of hourly precipitation extremes. *Nature Climate Change*, 7(1), 48–52. Available from: https://doi.org/10.1038/nclimate3168

Prein, A.F., Rasmussen, R.M., Wang, D. & Giangrande, S.E. (2021) Sensitivity of organized convective storms to model grid spacing in current and future climates. *Philosophical Transactions of the Royal Society A: Mathematical, Physical and Engineering Sciences*, 379(2195), 20190546. Available from: https://doi.org/10.1098/rsta.2019.0546

Pu, B. & Dickinson, R.E. (2014) Diurnal spatial variability of Great Plains summer precipitation related to the dynamics of the low-level jet. *Journal of the Atmospheric Sciences*. American Meteorological Society, 71(5), 1807–1817. Available from: https://doi.org/10.1175/JAS-D-13-0243.1

Rasmussen, K.L., Prein, A.F., Rasmussen, R.M., Ikeda, K. & Liu, C. (2020) Changes in the convective population and thermodynamic environments in convection-permitting regional climate simulations over the United States. *Climate Dynamics*, 55(1), 383–408. Available from: https://doi.org/10.1007/s00382-017-4000-7

Reidmiller, D.R., Avery, C.W., Easterling, D.R., Kunkel, K.E., Lewis, K.L.M., Maycock, T.K. et al. (2018) Impacts, Risks, and Adaptation in the United States: The Fourth National Climate Assessment, *Volume II*. U.S. Global Change Research Program.

Rogash, J.A. & Racy, J. (2002) Some meteorological characteristics of significant tornado events occurring in proximity to flash flooding. *Weather and Forecasting*, 17(1), 155–159. Available from: https://doi.org/10.1175/1520-0434(2002)017<0155:SMCOST>2.0.CO;2

Rogash, J.A. & Smith, R.D. (2000) Multiscale overview of a violent tornado outbreak with attendant flash flooding. *Weather and Forecasting*, 15(4), 416–431. Available from: https://doi.org/10.1175/1520-0434(2000)015<0416:MOOAVT>2.0.CO;2

Saltikoff, E., Friedrich, K., Soderholm, J., Lengfeld, K., Nelson, B., Becker, A. et al. (2019) An overview of using weather radar for climatological studies: successes, challenges, and potential. *Bulletin of the American Meteorological Society*, 100(9), 1739–1752. Available from: https://doi.org/10.1175/BAMS-D-18-0166.1

Schenkman, A.D. & Xue, M. (2016) Bow-echo mesovortices: A review. *Atmospheric Research*, 170, 1–13. Available from: https://doi.org/10.1016/j.atmosres.2015.11.003

Schumacher, R.S. (2015) Resolution dependence of initiation and upscale growth of deep convection in convection-allowing forecasts of the 31 May–1 June 2013 supercell and MCS. *Monthly Weather Review*, 143(11), 4331–4354. Available from: https://doi.org/10.1175/MWR-D-15-0179.1

Schwartz, C.S., Kain, J.S., Weiss, S.J., Xue, M., Bright, D.R., Kong, F. et al. (2009) Next-day convection-allowing WRF model guidance: A second look at 2-km versus 4-km grid spacing. *Monthly Weather Review*, 137(10), 3351–3372. Available from: https://doi.org/10.1175/2009MWR2924.1

Sheffield, J. & Wood, E.F. (2008) Projected changes in drought occurrence under future global warming from multi-model, multi-scenario, IPCC AR4 simulations. *Climate Dynamics*, 31(1), 79–105. Available from: https://doi.org/10.1007/s00382-007-0340-z

Sheridan, S.C. (2002) The redevelopment of a weather-type classification scheme for North America. *International Journal of Climatology: A Journal of the Royal Meteorological Society*, 22(1), 51–68.

Skamarock, W.C., Klemp, J.B., Dudhia, J., Gill, D.O., Liu, Z., Berner, J. et al. (2019) A description of the advanced research WRF model version 4. UCAR/NCAR.

Smith, B.T., Thompson, R.L., Grams, J.S., Broyles, C. & Brooks, H.E. (2012) Convective modes for significant severe thunderstorms in the contiguous United States. Part I: storm classification and climatology. *Weather and Forecasting*, 27(5), 1114–1135. Available from: https://doi.org/10.1175/WAF-D-11-00115.1

Smith, J.A., Baeck, M.L., Zhang, Y. & Doswell, C.A. (2001) Extreme rainfall and flooding from supercell thunderstorms. *Journal of Hydrometeorology*, 2(5), 469–489. Available from: https://doi.org/10.1175/1525-7541(2001)002<0469:ERAFFS>2.0.CO;2

Smith, J.A., Cox, A.A., Baeck, M.L., Yang, L. & Bates, P. (2018) Strange floods: the upper tail of flood peaks in the United States. *Water Resources Research*, 54(9), 6510–6542. Available from: https://doi.org/10.1029/2018WR022539

Sobash, R.A. & Kain, J.S. (2017) Seasonal variations in severe weather forecast skill in an experimental convection-allowing model. *Weather and Forecasting*, 32(5), 1885–1902. Available from: https://doi.org/10.1175/WAF-D-17-0043.1

Sobash, R.A., Kain, J.S., Bright, D.R., Dean, A.R., Coniglio, M.C. & Weiss, S.J. (2011) Probabilistic forecast guidance for severe thunderstorms based on the identification of extreme phenomena in convection-allowing model forecasts. *Weather and Forecasting*, 26(5), 714–728. Available from: https://doi.org/10.1175/WAF-D-10-05046.1

Sobash, R.A., Romine, G.S., Schwartz, C.S., Gagne, D.J. & Weisman, M.L. (2016) Explicit forecasts of low-level rotation from convection-allowing models for next-day tornado prediction. *Weather and Forecasting*, 31(5), 1591–1614. Available from: https://doi.org/10.1175/WAF-D-16-0073.1

Sobash, R.A., Schwartz, C.S., Romine, G.S., Fossell, K.R. & Weisman, M.L. (2016) Severe weather prediction using storm surrogates from an ensemble forecasting system. *Weather and Forecasting*, 31(1), 255–271. Available from: https://doi.org/10.1175/WAF-D-15-0138.1

Strader, S.M. & Ashley, W.S. (2015) The expanding bull's-eye effect. *Weatherwise*, 68(5), 23–29. Available from: https://doi.org/10.1080/00431672.2015.1067108

Taszarek, M., Allen, J.T., Brooks, H.E., Pilguj, N. & Czernecki, B. (2021) Differing trends in United States and European severe thunderstorm environments in a warming climate. *Bulletin of the American Meteorological Society*, 102(2), E296–E322. Available from: https://doi.org/10.1175/BAMS-D-20-0004.1

Taszarek, M., Allen, J.T., Púčik, T., Hoogewind, K.A. & Brooks, H.E. (2020) Severe convective storms across Europe and the United States. Part II: ERA5 environments associated with lightning, Large hail, severe wind, and tornadoes. *Journal of Climate*, 33(23), 10263–10286. Available from: https://doi.org/10.1175/JCLI-D-20-0346.1

Taylor, K.E., Stouffer, R.J. & Meehl, G.A. (2012) An overview of CMIP5 and the experiment design. *Bulletin of the American Meteorological Society*, 93(4), 485–498. Available from: https://doi.org/10.1175/BAMS-D-11-00094.1

Tebaldi, C., Hayhoe, K., Arblaster, J.M. & Meehl, G.A. (2006) Going to the extremes. *Climatic Change*, 79(3), 185–211. Available from: https://doi.org/10.1007/s10584-006-9051-4

Thompson, G., Field, P.R., Rasmussen, R.M. & Hall, W.D. (2008) Explicit forecasts of winter precipitation using an improved bulk microphysics scheme. Part II: implementation of a new snow parameterization. *Monthly Weather Review*, 136(12), 5095–5115. Available from: https://doi.org/10.1175/2008MWR2387.1

Tippett, M.K., Allen, J.T., Gensini, V.A. & Brooks, H.E. (2015) Climate and hazardous convective weather. *Current Climate Change Reports*, 1(2), 60–73. Available from: https://doi.org/10.1007/s40641-015-0006-6

Trapp, R.J. & Hoogewind, K.A. (2016) The realization of extreme tornadic storm events under future anthropogenic climate change. *Journal of Climate*, 29(14), 5251–5265. Available from: https://doi.org/10.1175/JCLI-D-15-0623.1

Trapp, R.J., Hoogewind, K.A. & Lasher-Trapp, S. (2019) Future changes in hail occurrence in the United States determined through convection-permitting dynamical downscaling. *Journal of Climate*, 32(17), 5493–5509. Available from: https://doi.org/10.1175/JCLI-D-18-0740.1

Trapp, R.J., Robinson, E.D., Baldwin, M.E., Diffenbaugh, N.S. & Schwedler, B.R.J. (2011) Regional climate of hazardous convective weather through high-resolution dynamical downscaling. *Climate Dynamics*, 37(3), 677–688. Available from: https://doi.org/10.1007/s00382-010-0826-y

Trapp, R.J. & Weisman, M.L. (2003) Low-level mesovortices within squall lines and bow echoes. Part II: their genesis and implications. *Monthly Weather Review*, 131(11), 2804–2823. Available from: https://doi.org/10.1175/1520-0493(2003)131<2804:LMWSLA>2.0.CO;2

Trenberth, K.E. (1999) Conceptual framework for changes of extremes of the hydrological cycle with climate change. In: Karl, T.R., Nicholls, N. & Ghazi, A. (Eds.) *Weather and climate extremes*. Dordrecht, Netherlands: Springer, pp. 327–339.

Trenberth, K.E., Dai, A., Rasmussen, R.M. & Parsons, D.B. (2003) The changing character of precipitation. *Bulletin of the American Meteorological Society*, 84(9), 1205–1218. Available from: https://doi.org/10.1175/BAMS-84-9-1205

Verrelle, A., Ricard, D. & Lac, C. (2015) Sensitivity of high-resolution idealized simulations of thunderstorms to horizontal resolution and turbulence parametrization. *Quarterly Journal of the Royal Meteorological Society*, 141(687), 433–448. Available from: https://doi.org/10.1002/qj.2363

Wallace, J.M. (1975) Diurnal variations in precipitation and thunderstorm frequency over the conterminous United States. *Monthly Weather Review*, 103(5), 406–419. Available from: https://doi.org/10.1175/1520-0493(1975)103<0406:DVIPAT>2.0.CO;2

Weaver, S.J., Baxter, S. & Kumar, A. (2012) Climatic role of north American low-level jets on U.S. regional tornado activity. *Journal of Climate*, 25(19), 6666–6683. Available from: https://doi.org/10.1175/JCLI-D-11-00568.1

Weisman, M.L., Skamarock, W.C. & Klemp, J.B. (1997) The resolution dependence of explicitly modeled convective systems. *Monthly Weather Review*, 125(4), 527–548. Available from: https://doi.org/10.1175/1520-0493(1997)125<0527:TRDOEM>2.0.CO;2

Weisman, M.L. & Trapp, R.J. (2003) Low-level mesovortices within squall lines and bow echoes. Part I: overview and dependence on environmental shear. *Monthly Weather Review*, 131(11), 2779–2803. Available from: https://doi.org/10.1175/1520-0493(2003)131<2779:LMWSLA>2.0.CO;2

WMO. (1986) *Manual for estimation of probable maximum precipitation*. 2d ed. WMO No. 332, 250 pp.

Wood, V.T., Brown, R.A. & Burgess, D.W. (1996) Duration and movement of mesocyclones associated with southern Great Plains thunderstorms. *Monthly Weather Review*, 124(1), 97–101. Available from: https://doi.org/10.1175/1520-0493(1996)124<0097:DAMOMA>2.0.CO;2

Zhang, G.J. (2009) Effects of entrainment on convective available potential energy and closure assumptions in convection parameterization. *Journal of Geophysical Research: Atmospheres*, 114(D7), 1–12. Available from: https://doi.org/10.1029/2008JD010976

Zhu, J. (2013) Impact of climate change on extreme rainfall across the United States. *Journal of Hydrologic Engineering*, 18(10), 1301–1309. Available from: https://doi.org/10.1061/(ASCE)HE.1943-5584.0000725

Zhu, J., Forsee, W., Schumer, R. & Gautam, M. (2013) Future projections and uncertainty assessment of extreme rainfall intensity in the United States from an ensemble of climate models. *Climatic Change*, 118(2), 469–485. Available from: https://doi.org/10.1007/s10584-012-0639-6

SUPPORTING INFORMATION

Additional supporting information can be found online in the Supporting Information section at the end of this article.

How to cite this article: Zeeb, A. W., Ashley, W. S., Haberlie, A. M., Gensini, V. A., & Michaelis, A. C. (2024). Supercell precipitation contribution to the United States hydroclimate. *International Journal of Climatology*, 1–24. https://doi.org/10.1002/joc.8395